NASA Technical Memorandum 87787

Cross Sections for Production of the 15.10-MeV and Other Astrophysically Significant Gamma-Ray Lines Through Excitation and Spallation of ^{12}C and ^{16}O With Protons

F. L. Lang, C. W. Werntz,
C. J. Crannell, J. I. Trombka,
and C. C. Chang

SEPTEMBER 1986

NASA

NASA Technical Memorandum 87787

Cross Sections for Production of the 15.10-MeV and Other Astrophysically Significant Gamma-Ray Lines Through Excitation and Spallation of ^{12}C and ^{16}O With Protons

F. L. Lang and C. W. Werntz
The Catholic University of America
Washington, D.C.

C. J. Crannell and J. I. Trombka
Goddard Space Flight Center
Greenbelt, Maryland

C. C. Chang
University of Maryland
College Park, Maryland

National Aeronautics
and Space Administration

**Scientific and Technical
Information Branch**

1986

I. INTRODUCTION

Nuclear gamma-ray line emission provides the most direct evidence available for the investigation of mechanisms by which protons and other ions are accelerated and interact in solar flares. Gamma rays, unlike charged particles, are unaffected by solar magnetic fields and thus carry unaltered information on characteristics of the accelerated-particle population as well as on the isotopic composition of the ambient medium in which the energetic particles interact. The current status of these investigations is presented in a review by Chupp.[1] The first definitive detection of nuclear lines from solar flares, reported by Chupp *et al.*,[2] was achieved with two flares on 1972 August 4 and 7. This stimulated renewed interest in previously published theoretical predictions.[3] Extensive observations obtained during the present solar cycle, together with new, detailed theoretical calculations, modified and clarified these earlier concepts.

Because most nuclear levels above 8 MeV are particle unstable and lead to little or no gamma-ray emission, studies of nuclear line emission from solar flares have focused on the energy range below 8 MeV. There is, however, unique and valuable information to be learned from observations of high-energy line emission. For example, a pair of gamma-ray lines from states with widely separated production thresholds can provide a measure of the spectrum of particles accelerated in a flare. The most promising candidate states are the 2^+, T = 0 level at 4.439 MeV and the 1^+, T = 1 level at 15.11 MeV, both in ^{12}C.[4] However, both excited states can be produced by spallation reactions with ^{16}O as well as by inelastic (p,p′) scattering from ^{12}C. If the ratio of the gamma-ray production cross sections for the two lines differs for the two nuclei, then the flux ratio of the two lines in solar flares is dependent on the abundance as well as the proton spectrum.

For the particular case of the carbon line pair from solar flares, production by spallation reactions with ^{16}O, which is more abundant in the solar photosphere than ^{12}C by a factor of 2,[5] contributes significantly to the line fluences. At the time the present experiment was performed, gamma-ray production cross sections for the reaction $^{16}O(p,x\,\gamma_{4.438})^{12}C$ had been measured,[6,7] and the results suggested that this process contributes more to the observed flux of 4.438-MeV gamma rays from flares than does the direct excitation of carbon. Preliminary measurements of the $^{16}O(p,x\,\gamma_{15.10})^{12}C$ reaction[8] suggested that the flux ratios of the 15.10-MeV to the 4.438-MeV line were comparable for the two nuclei. For purposes of calculations relating the accelerated particle spectral index to the ratio of the net fluences in the two lines, Crannell, Crannell, and Ramaty[4] assumed that the ratios were identical for the two nuclei. The actual values of the flux ratios are required for the interpretation of any solar flare observations, and the confidence with which they are known sets the limits on their utility as solar flare diagnostics. In the present work, measurements of the gamma-ray production cross section for the reaction $^{16}O(p,x\,\gamma_{15.10})^{12}C$ are reported.

The gamma-ray production cross section for the lower energy lines observed in the present work are important for planetary physics applications as well. Future planetary missions such as the Mars Observer will carry high-resolution gamma-ray spectrometers. The determination of surface abundances from observed spectra will depend on an accurate knowledge of these and other cross sections.

Measurements of the differential gamma-ray production cross sections were obtained using the University of Maryland cyclotron at three incident proton energies and for five gamma-ray observation angles at each energy. The cyclotron runs on which all results reported here are based were carried out in August 1979, ten months before the facility was officially closed. The gamma rays were measured with a high-purity germanium (HPGe) semiconductor detector. Spectra, covering the energy range from 50 keV to 20 MeV, were obtained with two targets for each energy and angle. A beryllium oxide target was employed for the oxygen cross section. A polyethelene target was employed to obtain measurements of the known carbon cross sections so that cross sections in oxygen could be determined as ratios to the corresponding cross sections in carbon, thus

eliminating the effects of uncertainties in the detector efficiency from the desired measurements.

The measurements obtained in the present work were employed in two different ways to determine estimates of the gamma-ray production cross sections. First, cross sections were calculated from these measurements using detector efficiencies calculated with the Monte Carlo technique of Seltzer.[9] Second, normalization factors were determined from a compilation of cross sections reported both for inelastic particle scattering experiments and for gamma-ray production measurements. Various discrepancies were encountered in previously reported results. The results reported here include the best estimates of a self-consistent resolution of these discrepancies. A major conclusion of this work, however, is that uncertainties in many of the cross sections are large compared to the accuracy desired for the determination of spectral parameters and isotopic abundances in solar flares and other astrophysical settings.

The measured spectra exhibit a much richer population of lines and features than would be expected from the level structure of individual target nuclei. The actual spectra are enriched and complicated by gamma rays emitted from numerous and abundantly produced spallation products. Ideally, these spectra should be measured with a detector having a high photopeak efficiency over the full energy range and a spectral resolution finer than the narrowest line to be resolved. The actual detector employed was one of the largest of its kind available at the time. Despite this fact, difficulties were encountered because its size was such that the first and second escape peaks were comparable to or greater than the photopeaks for the principal lines of interest. The fine resolution of the HPGe detector was very important in enabling individual lines to be resolved and spectral features of the broad lines of interest to be determined in detail. In portions of the spectrum in which blending with various photopeaks and escape peaks occurred, determination of the cross sections for Doppler-broadened lines required knowledge of their detailed spectral shapes.

The instrumentation and experimental techniques employed in the present work, including descriptions of the proton beam, the detector, and some of the background reduction techniques, are discussed in the following section. Knowledge of the shape of the 4.438-MeV line from ^{16}O was required for the calculation of the corresponding gamma-ray production cross section. In Sec. III, a method for determining the theoretical shapes of the 4.438-MeV line for both targets is described. The Doppler broadened shapes depend strongly on the angle of observation with respect to the proton beam direction. The question of whether there are preferential directions for the velocities of high energy protons or heavy ions at a solar flare site can perhaps be answered by a comparison of laboratory and solar gamma-ray line shapes. The analytic techniques used to determine the desired gamma-ray production cross sections from measured spectra are described in Sec. IV. In Sec. V results for the 15.10- and 4.438-MeV gamma-ray production cross sections are presented for both targets. In addition, the first resolved measurements of the gamma-ray production cross sections for the reactions $^{16}O(p,2p\,\gamma_{5.269})^{15}N$, $^{16}O(p,x\,\gamma_{5.240})^{15}O$, $^{16}O(p,x\,\gamma_{5.105})^{14}N$, $^{16}O(p,x\,\gamma_{2.793})^{14}N^*(2.313)$, $^{16}O(p,p'\gamma_{2.740})^{16}O^*(6.130)$, $^{16}O(p,x\,\gamma_{2.313})^{14}N$, and $^{12}C(p,x\,\gamma_{2.000})^{11}C$ are reported. The gamma-ray lines from the reactions $^{12}C(p,x\,\gamma_{2.154})^{10}B$ and $^{12}C(p,2p\,\gamma_{2.124})^{11}B$ could not be resolved. Results for these lines, therefore, are presented as a sum of the cross sections. Section V concludes with a summary of the results obtained to date and the remaining related requirements for astrophysical applications. Finally, assistance provided for this effort is gratefully acknowledged in Sec. VI.

II. EXPERIMENTAL METHOD

The data presented in this paper were obtained using the University of Maryland Sectored Isochronous Cyclotron Facility at a low background station especially designed for gamma-ray measurements. For this experiment, beams of 40-, 65-, and 85-MeV protons generated with the cyclotron were directed at three solid

targets. Pulse-height spectra were obtained with a high-purity germanium semiconductor at 70, 90, 110, 125, and 140 degrees relative to the direction of the incident beam for each proton energy.

The proton beam was pulsed, with a width of 1 ns at a repetition rate determined by the radio frequency of the cyclotron (one pulse every 60 to 90 ns depending on the proton energy). This allowed the effects of most background neutrons and gamma rays to be separated on the basis of the timing of the detector events relative to the radio-frequency (rf) pulse. The total beam current was measured with a Faraday cup attached to the beam line downstream of the target chamber. The beam line, target, and gamma-ray detector arrangement are shown schematically in Fig. 1.

Thin foils of polyethylene (CH_2), beryllium oxide (BeO), and beryllium (Be) were employed as targets. Each of these foils was held in an aluminum target frame which comprised a remotely changeable, three-element target ladder oriented at 45 degrees to the incident beam. At 45 degrees, the target angle employed, the CH_2, BeO, and Be targets presented thicknesses of 0.018 $\pm$ 0.002 g/cm^2 (^{12}C), 0.050 $\pm$ 0.005 g/cm^2 (^{16}O), and 0.018 $\pm$ 0.002 g/cm^2 (Be) to the proton beam, respectively. Because no intense gamma-ray lines arise from proton interactions with beryllium, the pulse-height spectra obtained with the beryllium target in place were used only to verify that the proton beam was not hitting the aluminum target frame.

The gamma rays were detected with a high-resolution semiconductor device comprised of high-purity germanium (HPGe) located 1.8 meters from the target. The HPGe detector is a cylinder 58 mm in diameter by 46 mm in height. Due to neutron damage sustained prior to these measurements, this detector had a relatively poor spectral resolution of about 7 keV (FWHM) at 1.332 MeV. As located, it subtended a solid angle of 0.72 $\pm$ 0.02 msr.

Background events resulting from neutrons, protons, and other particles incident on the detector produced many of the observed events. Background events due to protons which scattered from the target and charged spallation products produced in the target were reduced by placing beryllium shielding 14.2 $\pm$ 0.3 g/cm^2 thick between the target and the detector.

A time-of-flight window was used to eliminate most of the neutron events, the major source of background in the raw, ungated pulse-height spectra. Figure 2 shows a sample arrival-time spectrum, such as was used to set the window. Plotted, on a semi-log scale, are the counts as a function of the difference in time between the HPGe detector signal and the rf timing pulse associated with the accelerator. The arrival time of the prompt gamma rays spans only twenty percent of the 60 ns between beam bursts. With an acceptance window set to correspond to the arrival time of the prompt gamma rays of interest, all of which originate from states with lifetimes less than 10 ns, most of the neutron background, as well as most of the very long-lived radioactive-decay gamma rays (lifetime $>$ 10 ns), were eliminated. Events which satisfied the timing and energy-threshold criteria were selected for further analysis. Figures 3(a)–3(d) show pulse-height spectra with and without this neutron suppression. An improvement by more than an order of magnitude can be seen in the signal-to-noise ratio.

The detector gain was very stable over all runs with a standard deviation of 0.2%. This was determined by comparison of the centroid of the 6.129-MeV ^{16}O photopeak and the centroid of the 4.218-MeV ^{15}O second escape peak for all BeO target runs. The relatively long lifetime ($\tau > 1$ ps) of these two states allowed the excited nuclei to come to rest in the solid targets. Thus, the corresponding gamma-ray lines are intrinsically narrow. Because there are relatively few narrow lines observed in our spectra, these two lines proved to be very useful for monitoring the gain of the detector.

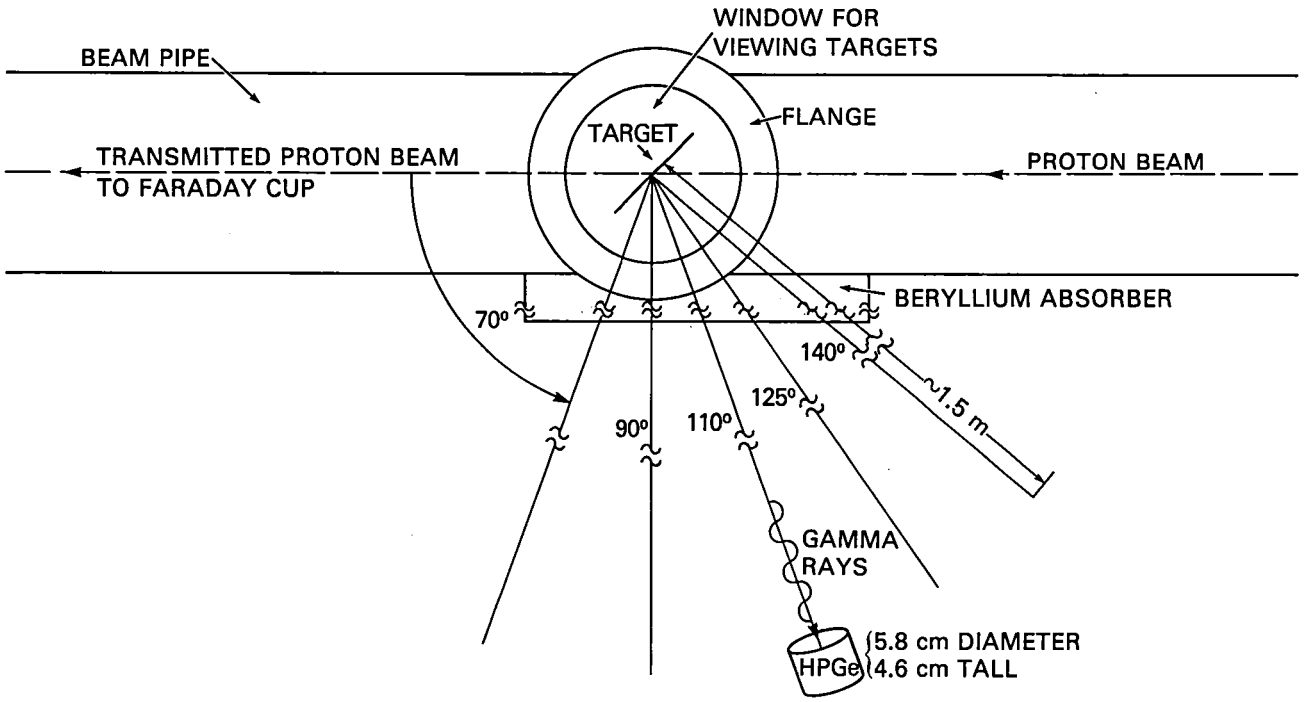

Figure 1. This is a schematic diagram illustrating the experimental setup as seen from above. The proton beam enters from the right. All but a negligibly small fraction of the incident protons pass through the thin target and are collected by the Faraday cup to measure the incident flux. A small fraction of the protons interact in the target, and the resulting gamma rays and nuclear debris scatter in all directions. A subset of the interaction products are detected with the high-purity Germanium detector.

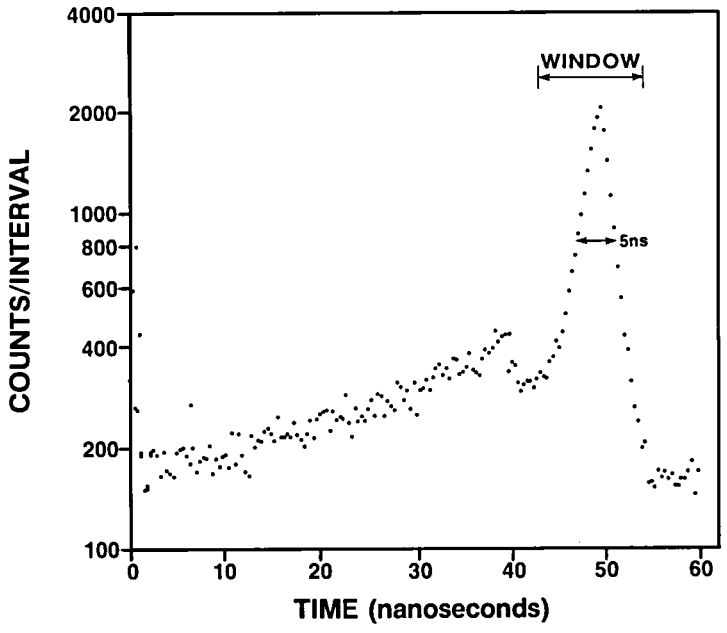

Figure 2. Arrival time spectrum of events detected with the high-purity germanium detector (HPGe). Time is measured from a trigger generated by an event in the germanium detector to the next of the periodic pulses which trigger the incident beam. The vertical scale is the number of HPGe events per time interval.

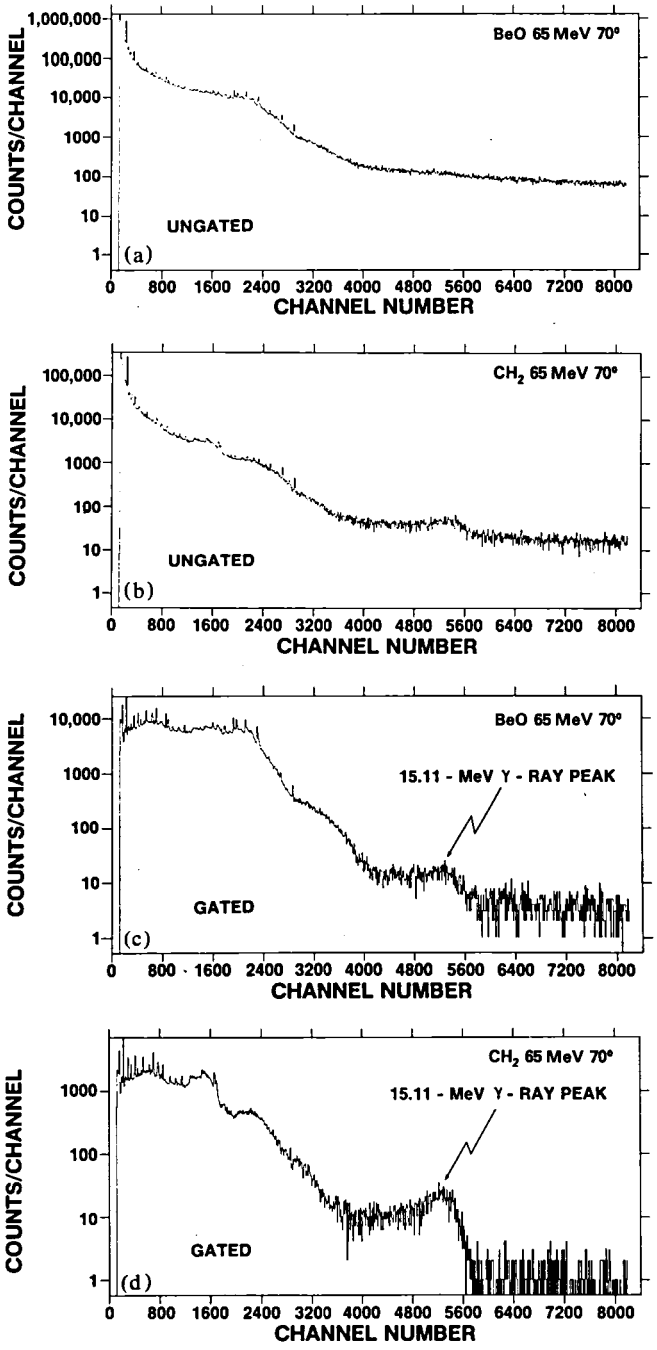

Figure 3. (a) A typical total pulse-height spectrum for 65-MeV protons incident on the BeO target. It was measured at 70 degrees to the proton beam for approximately 1 hour. This spectrum is dominated by the large background of neutrons and delayed gamma rays. Each histogram bin gives the total counts in eight raw pulse-height channels. (b) A typical total pulse-height spectrum for 65-MeV protons incident on the CH_2 target. It was measured at 70 degrees to the proton beam for approximately 40 minutes. This spectrum is dominated by the large background of neutrons and delayed gamma rays. Each histogram bin gives the total counts in eight raw pulse-height channels. (c) The pulse-height spectrum of events selected from the spectrum shown in (a) by imposing the TAC window constraint. (d) The pulse-height spectrum of events selected from the spectrum shown in (b) by imposing the TAC window constraint.

III. THEORETICAL LINE SHAPES

III.A. $^{12}C(p,p'\gamma_{4.438})^{12}C$ line shape

The width of a gamma-ray line produced in a (p,p'γ) reaction depends critically on whether the lifetime of the gamma-ray emitting state is less than or greater than the slowing down time of the recoiling ion in the target material. In a solid target, if the lifetime is of the order of picoseconds or longer there will be no Doppler broadening and the transition gamma rays will be observed as a narrow line. On the other hand, transitions of states with femtosecond or shorter lifetimes give rise to broad lines whose shapes are characteristic of the kinetics of the originating nuclear reaction. In order to extract the strength of a given transition from an experimental spectrum in which the background can change over the width of such a line, it is advantageous to have a model for calculating the shape of the line. This can greatly improve the accuracy with which the gamma-ray production cross section can be determined.

These considerations are particularly relevant to the $^{12}C(p,p'\gamma_{4.438})^{12}C$ and $^{16}O(p,x\ \gamma_{4.438})^{12}C$ reactions. In the former reaction, the gamma-ray line observed at right angles in the center-of-momentum frame to the initial proton beam direction is split into two symmetric peaks. This so-called "coherent Doppler effect" was observed and quantitatively explained by Kolata, Auble, and Galonsky.[10] A modified version of their theoretical treatment is presented here as preparation for a derivation of the shape of the same line produced by interactions in an ^{16}O target.

Consider the (p,p'γ) reaction in the center of momentum frame of the proton and target. Referring to Fig. 4, θ_c and ϕ_c are defined to be the scattering angles of the excited nucleus N* in the usual polar coordinates ($\theta_p = \pi - \theta_c$, where θ_c is the scattering angle of the incident nucleus with respect to the z axis). The vector $\bar{\beta}_c$ is the center of momentum velocity of N* in units of c. (A bar over a symbol, such as $\bar{v}$, indicates a vector quantity, while a caret over the same symbol indicates the associated unit vector.) The normal to the scattering plane is defined by $\hat{n} = \hat{k}_i \times \hat{k}_f$. The vector $\bar{k}_\gamma$ is the observed gamma-ray momentum whose direction is determined by the detector position.

For a fixed scattering plane, an observed gamma ray will have its energy Doppler shifted by an amount E_c to an energy $E = E_o + E_c$, where E_o is the gamma-ray energy in the rest frame of the excited nuclear state. Because of the small velocities involved, only terms linear in $\bar{\beta}_c$ need be retained and

$$E_c = E_o \bar{\beta}_c \cdot \hat{k}_\gamma. \tag{1}$$

The relative number of gamma rays with this Doppler shift is proportional to the differential cross section for producing an N* moving in the direction defined by θ_c and ϕ_c. The relative number also depends on the angle ϕ between the normal to the scattering plane and the gamma-ray direction, where

$$\cos(\phi) = \hat{k}_\gamma \cdot \hat{n} = \cos(\phi_c) * \sin(\theta_\gamma) \tag{2}$$

(see Fig. 4) because the angular distribution of gamma rays for a given θ_c is determined by the magnetic sublevel populations of the excited nuclear state referred to the axis $\hat{n}$.[10]

Let $N_c(\theta_\gamma,E_c)$ be defined to be the distribution function for the gamma rays with respect to the observation angle θ_γ and the shift energy E_c. Then $N_c(\theta_\gamma,E_c)$ can be expressed in terms of an integral over all scattering angles, weighted by the differential reaction cross section $\sigma(\theta_c)$, and restricted by a delta function imposing the relationship on the spectrum expressed in Eq. (1):

$$N_c(\theta_\gamma,E_c) = \iint d(\cos\theta_c)\, d\phi_c \sigma(\theta_c)\omega(\theta_c,\phi)\delta(E_c - E_o\bar{\beta}_c \cdot \hat{k}_\gamma). \tag{3}$$

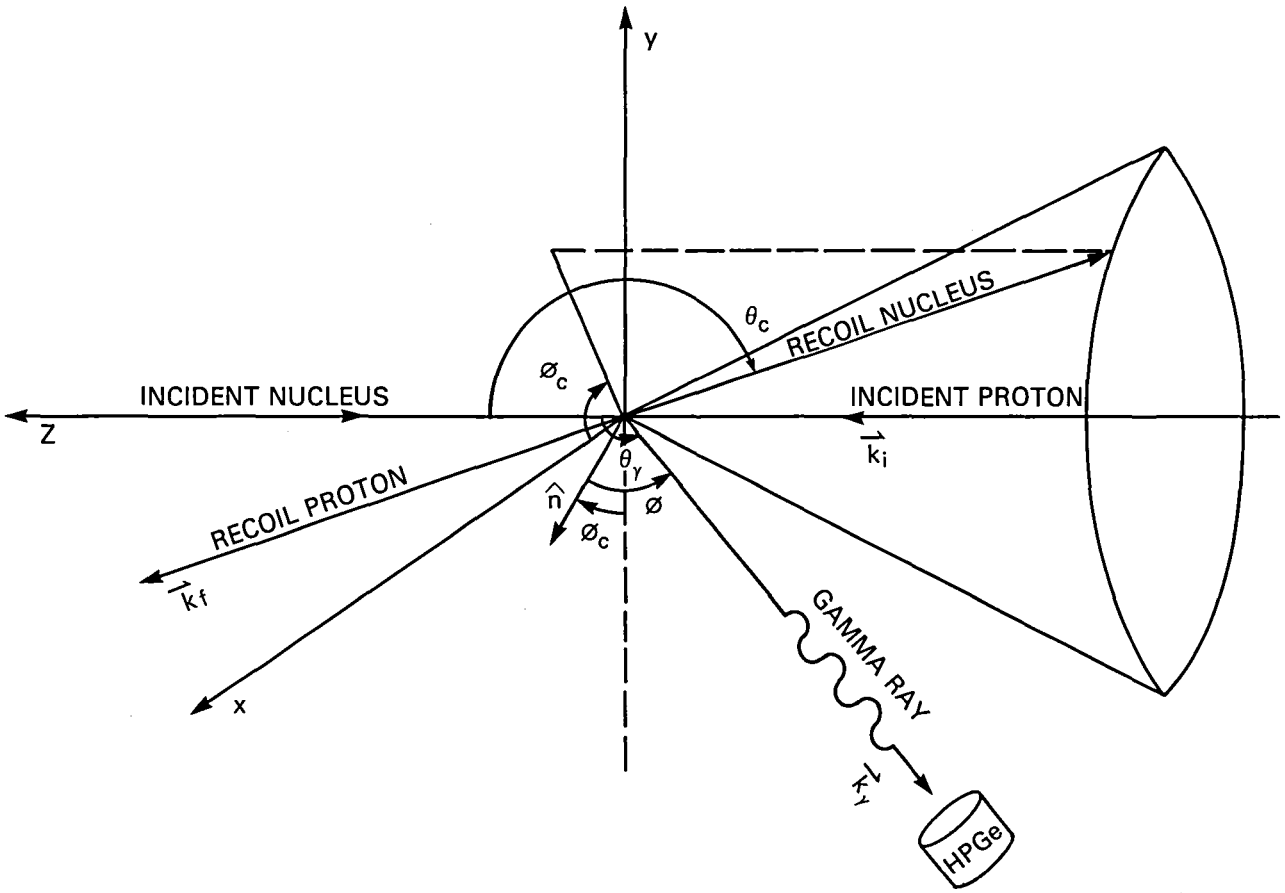

Figure 4. Center-of-momentum coordinate system for inelastic proton scattering. Protons enter from the right, target nuclei from the left. The vector $\hat{n}$ is defined by $\hat{k}_i \times \hat{k}_f$. The vector $\bar{k}_\gamma$ is the observed gamma-ray momentum, the direction of which is determined by the detector position. The final direction of the inelastically scattered nucleus is specified by the polar coordinates (θ_c,ϕ_c), where ϕ_c is measured from the normal to the detector-beam plane.

The function $\omega(\theta_c,\phi)$ describes the distribution of gamma rays relative to the quantization axis $\hat{n}$. The distribution depends on the magnetic substate populations P(m) and the multipolarity of the transition through the expression

$$\omega(\theta_c,\phi) \equiv \omega(\phi) = \sum_{m=-l}^{l} P(m) \parallel \bar{\chi}_l^m(\phi,\alpha) \parallel^2, \tag{4}$$

where the $\bar{\chi}_l^m(\phi,\alpha)$ are the vector spherical harmonics defined in Jackson;[11] α is the azimuthal angle of the gamma ray about $\hat{n}$, measured with respect to an axis in the scattering plane. By inspection, $\omega(\phi)$ is independent of α. Any dependence of P(m) on the nuclear scattering angle θ_c has been suppressed. Because a scalar, $\bar{J}_{N^*} \cdot (\bar{k}_i \times \bar{k}_f)$, linear in the angular momentum $\bar{J}_{N^*}$ of the excited nucleus can be constructed, the final nuclear state can be polarized along $\hat{n}$, i.e., $P(m) \neq P(-m)$. Nevertheless, with only a single multipole contributing, $\omega(\phi)$ is symmetric about the plane defined by $\phi = \pi/2$.

The delta function in Eq. (3) reduces the double integral to a single integral over θ_c where ϕ can be expressed as a function of θ_c, θ_γ, and E_c:

$$N_c(\theta_\gamma,E_c) = \int \frac{d(\cos\theta_c)\sigma(\theta_c)\omega(\phi[\theta_c,\theta_\gamma,E_c])}{[(E_o\beta_c \sin\theta_\gamma \sin\theta_c)^2 - (E_c - E_o\beta_c \cos\theta_\gamma \cos\theta_c)^2]^{1/2}}, \quad (5)$$

where

$$\cos\phi = [(E_o\beta_c \sin\theta_\gamma \sin\theta_c)^2 - (E_c - E_o\beta_c \cos\theta_\gamma \cos\theta_c)^2]^{1/2}/(E_o\beta_c \sin\theta_c), \quad (6)$$

and the integral in Eq. (5) is performed over values of θ_c such that the denominator is real. In order to understand how a double peak structure of the gamma-ray line can arise, consider the gamma-ray spectral distribution function for $\theta_\gamma = \pi/2$ and $E_c = 0$. If there is no Doppler shift, the gamma ray must have been emitted at right angles to the scattering plane so that $\hat{k}_\gamma \cdot \hat{n} = \pm 1$ and $\phi = 0, \pi$. Because $\omega(\phi) = \omega(\pi - \phi)$, the distribution function can be written as

$$N_c(\pi/2,0) = 2\int_{-1}^{+1} d(\cos\theta_c) \frac{\sigma(\theta_c)\omega(0)}{E_o\beta_c \sin\theta_c}. \quad (7)$$

If this is specialized to the case of interest, a $2^+ \rightarrow 0^+$ transition, both $\bar{\chi}_2^0(0,\alpha)$ and $\bar{\chi}_2^{\pm 2}(0,\alpha)$ are zero. If the m $= \pm 1$ sublevels are not populated by the $^{12}C(p,p'\gamma_{4.438})^{12}C$ reaction, $\omega(0) = 0$ and there are no gamma rays of energy E_o! That there are two mirror symmetric peaks for $\theta_\gamma = \pi/2$ is a special case of the more general symmetry obtainable from Eq. (5),

$$N_c(\theta_\gamma,E_c) = N_c(\pi - \theta_\gamma, -E_c). \quad (8)$$

Ramaty, Kozlovsky, and Lingenfelter[12] have reported that, at $\theta_\gamma = \pi/2$, a dip can occur at the center of the 4.438-MeV line from $^{12}C(p,p'\gamma_{4.438})^{12}C$, even for isotropic gamma-ray emission. By definition, isotropic emission occurs when all $2I + 1$ magnetic sublevels are equally populated. In this case, $P(m) = 1/(2I + 1)$, which leads to $\omega(\phi) = 1/(4\pi)$. The shape of this gamma-ray line has been computed by numerically integrating the right hand side of Eq. (5), using the $E_p = 50$ MeV data of Fannon, *et al.*[13] for the differential scattering cross sections, as well as the isotropic sublevel population distribution given by $P(m) = 1/(2I + 1) = 0.2$. This results in the line shape shown as the single broad peak of Fig. 5. When the line shape is computed using the sublevel population distribution reported as isotropic by Ramaty, Kozlovsky, and Lingenfelter[12] [$P(0) = 1/3$ and $P(m) = 1/6$ for $m = \pm 1, \pm 2$], a dip at the center of the line is obtained as shown in Fig. 5. This sublevel population distribution, however, does not correspond to isotropic gamma-ray emission.

In the present work, only the directions of the incoming proton and the outgoing 4.438-MeV gamma ray are observed. Because the emitting state has a definite parity, the angular distribution of gamma rays must be symmetric around $\theta_\gamma = \pi/2$. In the notation used here the number of gamma rays at a given angle, $N_c(\theta_\gamma)$, is obtained from the distribution function $N_c(\theta_\gamma,E_c)$ through integration over all values of E_c for which $N_c(\theta_\gamma,E_c)$ is non-zero:

$$N_c(\theta_\gamma) = \int dE_c N_c(\theta_\gamma,E_c). \quad (9)$$

Once again, by symmetry,

$$N_c(\theta_\gamma,E_c) = N_c(\pi - \theta_\gamma, -E_c), \quad (10)$$

so that

$$N_c(\theta_\gamma) = N_c(\pi - \theta_\gamma). \quad (11)$$

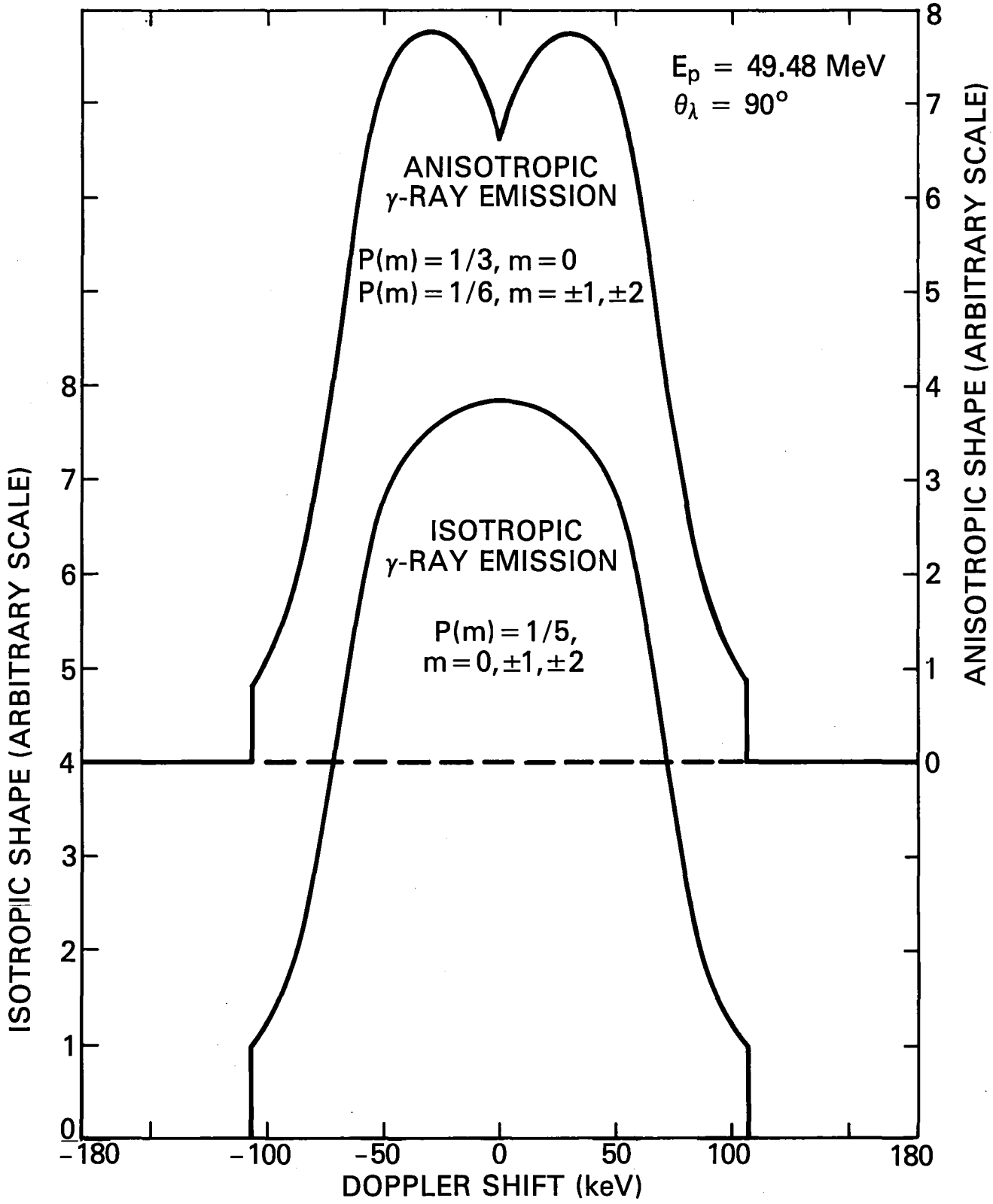

Figure 5. Line shapes for 4.438-MeV gamma rays from inelastic scattering of 49.48-MeV protons by ^{12}C measured 90° from the beam direction in laboratory coordinates. Shown are calculations for isotropic emission and for anisotropic emission on arbitrary scales.

The considerations just presented do not take into account the Doppler shift introduced by the transformation from the center of momentum to the laboratory frame. The distribution function with respect to angle θ'_γ and Doppler shift E'_c in the laboratory frame is defined through the relation

$$N(\theta'_\gamma,E'_c)\,\Delta\Omega'_\gamma\,\Delta E'_c = N_c(\theta_\gamma,E_c)\,\Delta\Omega_\gamma\,\Delta E_c. \tag{12}$$

The photon energy E' and angle θ'_γ are expressed in terms of the same quantities in the center of momentum frame through the standard equations

$$E' = \gamma_c E(1 + \beta_{cm}\cos\theta_\gamma) = E_o + E'_c \tag{13}$$

and

$$\tan\theta'_\gamma = \sin\theta_\gamma/[\gamma_c(\cos\theta_\gamma - \beta_{cm})]. \tag{14}$$

Here β_{cm} is the speed of the center of momentum frame, $\gamma_c = 1/\sqrt{1-\beta_{cm}^2}$, $\cos(\theta_\gamma) = \hat{\beta}_{cm}\cdot\hat{k}_\gamma$, and E'_c is the laboratory Doppler shift. For small β_{cm} (the case encountered in this experiment), $\gamma_c \approx 1$, $\theta_\gamma \approx \theta'_\gamma$, and $\Delta\Omega_\gamma \approx \Delta\Omega'_\gamma$, so that, to lowest order in β_{cm},

$$E'_c = E_c + \bar{\beta}_{cm}\cdot\hat{k}_\gamma = E_o(\bar{\beta}_c + \bar{\beta}_{cm})\cdot(\hat{k}_\gamma). \tag{15}$$

Then it follows that the laboratory distribution function $N(\theta'_\gamma,E'_c)$ can be determined to a good approximation from the center of momentum distribution function through the relationship

$$N(\theta'_\gamma,E'_c) = N_c(\theta_\gamma,E_c - \bar{\beta}_{cm}\cdot\bar{k}_\gamma). \tag{16}$$

III.B. $^{16}O(p,x\,\gamma_{4.438})^{12}C$ line shape

Both the 4.438- and the 15.10-MeV line of ^{12}C were produced by proton interactions in the BeO target. Both lines are broadened and required the use of a "template" to separate them from the background. The broadening of the 15.10-MeV line is due primarily to instrumental resolution, so the observed shape of the 15.10-MeV line with the ^{12}C target in place was used as a template (see Sec. IV.A.2). On the other hand, the shape of the 4.438-MeV line from the $^{16}O(p,x\,\gamma_{4.438})^{12}C$ reaction is influenced primarily by Doppler broadening, so the model for the $^{12}C^*(4.439)$ recoil derived in this section was adopted to allow computation of the intrinsic line shape.

A one-step model for $^{12}C^*$ production from protons on ^{16}O provides the most tractable equations for practical calculations. The ground state of ^{16}O can be rigorously expanded in a complete product set of twelve-body and four-body clusters:

$$|\Psi> = C_o\,|^{12}C + \alpha> + C_1\,|^{12}C^*(4.439) + \alpha> + \ldots. \tag{17}$$

The largest component is certainly the ^{12}C ground state plus an α in a relative s-state, while the $^{12}C^*(4.439)$ plus an α in a relative d-state is the next largest component.[14] In a one-step, or direct, process the desired final state is reached through a single interaction of the proton with one of the cluster components followed by the emission of the clusters which undergo at most elastic final-state interactions. If the proton excitations are restricted to one-step processes, $^{12}C^*(4.439)$ can be produced in several ways. One is through knocking the α out of ^{16}O leaving behind the $^{12}C^*$ residual nucleus with a probability proportional to $(C_1)^2$. Another is through exciting the ^{12}C component to $^{12}C^*$ and transferring to it enough recoil energy to eject it from the ^{16}O nucleus ($^{12}C^* + \alpha$ has a threshold energy of 11.6 MeV in ^{16}O).

For 40-MeV protons the condition that the final clusters undergo at most elastic final state interactions is not likely to be satisfied for either of the one-step processes just described. In a collision of the proton with either the mass-4 or mass-12 cluster there is no scattering angle for which sufficient energy can be transferred to either cluster to insure that the excitation energy will be above the resonance region of ^{16}O (which extends up to 30 MeV). Thus, coupling to other final state channels occurs in a manner characteristic of individual resonances. This means that the $^{12}C^* + \alpha$ will be emitted through the decay of resonant ^{16}O states in the predominantly $T = 0$ region of $^{16}O^*$. Thus, one can anticipate that a more useful description of this process is that of excitation of states in ^{16}O through (p,p′) and the subsequent decay of these states through the $^{12}C^* + \alpha$ channel, that is

$$^{16}O(p,p')^{16}O^*(E_N) \rightarrow {}^{12}C^*(4.439) + \alpha. \tag{18}$$

The dominance of what can be termed a multi-step process of formation of $^{12}C^*(4.439)$ has been confirmed by Epstein *et al.*[15] who worked with 46.8-MeV protons. Studying the $^{16}O(p,p'\alpha)^{12}C^*(4.439)$ reaction through measurements of the energies of protons and alpha particles in coincidence at fixed laboratory angles, they concluded that one-step (or direct) processes played virtually no role. The principal ^{16}O excited states through which the reaction proceeds have been identified from an examination of the cross section plotted as a function of the energy of the recoil proton, as presented in Figs. 9 and 10 of Epstein *et al.* The one-step process, as opposed to the multi-step process, is probably not significant below proton energies of about 100 MeV, at which energy the production of $^{12}C^*(4.439)$ has been observed to occur weakly through quasi-free p-α scattering.[14] Note that $^{12}C^*(15.11)$ cannot be produced through quasi-free p-α scattering because of isospin conservation in the ^{16}O ground state. In the analysis of the 4.438-MeV line that follows, its production is treated as a multi-step process.

In order to calculate the Doppler broadened shape of the line, the problem is initially treated in the overall $^{16}O + p$ center of momentum frame. In the two step process described by Eq. (18), the recoil velocity of $^{12}C^*(4.439)$ is the sum of $\bar{\beta}_c(E_N)$, the velocity of the $^{16}O^*(E_N)$ in the overall center of momentum frame, and $\bar{\beta}(E_N)$, the velocity of the emitted $^{12}C^*(4.439)$ nucleus in the center of momentum frame of the recoiling $^{16}O^*(E_N)$. In the overall center of momentum frame, the distribution function for 4.438-MeV gamma rays being emitted in a direction θ_γ with a Doppler shift E_c following excitation of the ^{16}O target to an energy E_N is given by

$$N_c(\theta_\gamma,E_c,E_N) = \iint d\hat{\beta}_c\, d\bar{\beta}\, n(\hat{k}_\gamma,\hat{\beta}_c,\bar{\beta})\delta\{E_c - E_o[\bar{\beta}_c(E_N) + \bar{\beta}(E_N)]\}. \tag{19}$$

The function $n(\hat{k}_\gamma,\hat{\beta}_c,\bar{\beta})$ is proportional to the number of gamma rays emitted in the direction $\hat{k}_\gamma$ when the $^{12}C^*(4.439)$ recoils with velocity $\bar{\beta}_c(E_N) + \bar{\beta}(E_N)$.

A close examination of the present data for the Doppler broadened 4.438-MeV line reveals only a suggestion of the double peak structure that is observed when ^{12}C is the target. Therefore it is likely that the sum over many levels of different J^π is equivalent to isotropic decay of $^{16}O^*(E_N)$ through $^{12}C^*(4.439) + \alpha$ followed by isotropic emission of a gamma ray by the excited carbon nucleus. Then

$$n(\hat{k}_\gamma,\hat{\beta}_c,\bar{\beta}) \rightarrow \frac{\Gamma_{\alpha 1}(E_N)}{\Gamma_{tot}(E_N)}\,\sigma(\theta_c,E_N)\,\frac{1}{4\pi}\,\frac{\delta[\beta - \beta_m(E_N)]}{\beta_m^2(E_N)}\,\frac{1}{4\pi}, \tag{20}$$

where $\Gamma_{\alpha 1}(E_N)$ is the partial width for decay of the level through the $^{12}C^* + \alpha$ channel, $\Gamma_{tot}(E_N)$ is the total width of the level, $\sigma(\theta_c,E_N)$ is the differential cross section for the $^{16}O(p,p')^{16}O^*(E_N)$ reaction, and $\bar{\beta}_m(E_N)$ is the velocity of the $^{12}C^*(4.439)$ relative to the $^{16}O^*(E_N)$ center of momentum frame. The E_N may be considered to be discrete energies since the width of the states are small compared to their excitation energies.

The integration over $\bar{\beta}$ can be carried out analytically with the net result that the term

$$[(E_o\beta_c \sin\theta_\gamma \sin\theta_c)^2 - (E_c - E_o\beta_c \cos\theta_\gamma \cos\theta_c)^2]^{-1/2} \tag{21}$$

inside the integral of Eq. (5) is replaced by

$$\frac{[\sin^{-1}(y + f) - \sin^{-1}(y - f)]}{2\beta_m(E_N)E_o}, \tag{22}$$

where

$$y = \frac{E_c - E_o\beta_c \cos\theta_\gamma \cos\theta_c}{E_o\beta_c \sin\theta_\gamma \sin\theta_c} \tag{23}$$

and

$$f = \beta_m/[\beta_c \sin\theta_\gamma \sin\theta_c]. \tag{24}$$

It is understood that if the argument of either or both arcsine functions is ≤ -1 or $\geq +1$ they must be assigned the values $-\pi/2$ or $+\pi/2$, respectively, in order to satisfy the limits on the angular integration.

The gamma-ray distribution function given by Eq. (19) refers to the center of momentum frame of $^{16}O + p$ and to the contribution of a single ^{16}O excited state of energy E_N. The transformation to the laboratory frame is made in the same way as was carried out in deriving Eq. (16), and to get the contribution from all ^{16}O levels one must sum over all E_N. The working expression for the distribution of gamma ray energies is

$$N(\theta'_\gamma,E'_c) = \sum_N N_c(\theta_\gamma,E_c - \bar{\beta}_{cm} \cdot \bar{k}_\gamma,E_N). \tag{25}$$

In the above equation $\bar{\beta}_{cm}$ is the laboratory velocity of the $^{16}O + p$ center of momentum frame.

In order to use Eq. (25) to calculate the shape of the gamma-ray line, it is necessary to know the differential cross sections, $\sigma(\theta_c,E_N)$, for exciting states (through inelastic proton scattering) which have large widths for decay through $^{12}C^*(4.439) + \alpha$. Buenerd *et al.*[16] have published cross sections for $E_p = 45$ MeV, $\theta_{lab} = 40$ degrees. For $E_N \leq 16$ MeV the proton spectrum consists of relatively isolated peaks. Each peak can be associated with states seen in a recent high-resolution (e,e′) experiment[17] and with states tabulated by Ajzenberg-Selove.[18] Not only are the spins and isospins known but the ratios of the transition widths $\Gamma_{\alpha 1}$ to Γ_{tot} for each state are relatively well known. These data are summarized in Table I. States which are near enough to the inelastic scattering peaks in the proton spectrum to give contributions are enclosed within parentheses. For example, there is a strong indication from the data of Amos *et al.*[21] that at $E_p = 135$ MeV the 2^- state at 15.20 MeV rather than the 2^+ state at 15.26 MeV is strongly excited in (p,p′). In general, 1^-, 2^-, and 3^- states are much in evidence.

For excitation energies above 16 MeV, detailed information about particle widths of states is not available. Above 15.5 MeV the $^{16}O(p,p'\alpha)^{12}C^*(4.439)$ experiment of Epstein *et al.*[15] allows the identification of states which decay significantly through the $^{12}C^*(4.439) + \alpha_1$ channel, but a quantitative knowledge of $\Gamma_{\alpha 1}(E_N)/\Gamma_{tot}(E_N)$ is still missing. Without exception, these states can be correlated with strong peaks in the Buenerd *et al.*[16] spectrum, at least up to values of E_N of about 25.5 MeV, at which energy the spectrum becomes smooth. Amazingly, isolated peaks[15] (relatively weak, however) seen in $^{16}O(p,p'\alpha)^{12}C^*(4.439)$ can be identified as peaks seen in the reactions $^{13}C(^3He,\alpha\gamma_{15.10})^{12}C$,[23] $^{15}N(p,\alpha\gamma_{15.10})^{12}C$,[25] and $^{14}N(d,\alpha\gamma_{15.10})^{12}C$.[24] In Table I selected peaks from the $^{16}O(p,p')^{16}O^*$ spectra[16] and from the recently reported $^{16}O(e,e')^{16}O^*$ experiment[17] are correlated with the $^{16}O(p,p'\alpha)^{12}C^*(4.439)$ spectrum.[15] Where possible, these peaks have been identified with entries in the latest compilation of ^{16}O states by Ajzenberg-Selove.[18]

Table I. Excited states of ^{16}O which have significant widths for decay into $^{12}C^*(4.439) + \alpha_1$. In the first two columns, the excitation energies of all peaks seen from 11.6 to 15.5 MeV in the $^{16}O(p,p')^{16}O^*(E_N)$ reactions are listed. Energies of the same states, if observed in $^{16}O(e,e')^{16}O^*$ or tabulated in a compilation of levels, appear in the next two columns. The next two columns give the spin, parity, and isospin of each state and the ratio $\Gamma_{\alpha 1}/\Gamma_{tot}$. States which are near the (p,p') energies and may contribute some strength are in parentheses. States with 0.0 in the last column obviously do not contribute to $^{16}O(p,x\ \gamma_{4.438})^{12}C$. Above 15.5 MeV, the important states were observed directly in the $^{16}O(p,p'\alpha)^{12}C^*$ reaction. At the upper end of the excitation range are the states which have been observed also in reactions which lead to the decay of ^{16}O via the $^{12}C^*(15.11) + \alpha$ channel.

Production		Reaction /	Source			
$(p,p'\alpha_1)$[a] (MeV)	(p,p')[b] (MeV)	(e,e')[c] (MeV)	(Compilation)[d] (MeV)	J^π	T^d	$\frac{\Gamma_{\alpha 1}}{\Gamma_{tot}}$
	12.05	12.05	12.05	0^+	0	0.00[d]
	12.53	12.53	12.53	2^-	0	1.00[d]
	13.02	Not resolved	13.02	2^+	0	0.00[e]
		"	(13.12)	3^-	1	0.37[e]
	13.26	13.26	13.26	3^-	0	0.25[e]
		(13.87)	(13.87)	4^+	0	0.42[f]
	13.97	. . .	(13.98)	2^-		0.50[d]
		(14.03)	(14.03)	0^+		0.00[f]
		(15.20)	(15.20)	2^-	(0,1)[g]	0.22[h]
	15.27	. . .	15.26	2^+	0	0.91[h]
15.5	15.50	15.41	15.41	3^-	0	0.25
17.2			17.20	2^+	0	
	17.25	17.27–.35	17.27	1^-	1	
		17.79	17.77	4^-	0	
17:9	17.88	17.88	18.02	4^+	0	
			18.46	2^+	0	
18.6	18.60	18.50	18.6	$(1^-,5^-)$		
		18.64	18.6	(4^+)		
		18.98	18.98	4^-	1	
19.1	19.1	19.21	19.21	3^-	1	
		20.51	20.50			
20.6	20.56		20.54	5^-		
			20.56			
21.8	21.8	21.7	(21.78)	3^-		
22.4	22.4		22.4	1^-	1	
24.0	24.0		24.0	1^-	1	
24.7[ij]			24.76	$(2^+,4^+)$	1	
25.2[k]			25.2		1	
26.0[ijk]			26.0	1^-	1	
27.1[ijk]			27.3	$(2^+,4^+)$	1	
28.0[ijk]						
29.6[j]			29.7		1	

[a] Reference 15.
[b] Reference 16.
[c] Reference 17.
[d] Reference 18.
[e] Reference 19.
[f] Reference 20.
[g] Reference 21.
[h] Reference 22.
[i] Reference 23.
[j] Reference 24.
[k] Reference 25.

IV. CALCULATIONAL TECHNIQUES

Each gamma-ray line of interest incident on the detector produced one or more recognizable features in the pulse-height spectrum. The gamma-ray line area, or simply the area, associated with a spectral feature is defined to be the number of pulse-height events comprising the feature. The differential gamma-ray production cross section for the incident line that produces the feature is then proportional to the measured area and inversely proportional to the absolute detector efficiency for converting an incident gamma ray in the line to an event in that feature. A brief description of the observed features, the techniques employed to determine the area of each selected feature, the absolute detector efficiencies, and the computation of the cross sections from the measured areas is presented in this section.

IV.A. Determination of gamma-ray line areas from measured spectra

IV.A.1. Spectral features

A monochromatic beam of gamma rays incident on a germanium detector will produce one or more prominent features in the measured pulse-height spectrum. The pulse-height events comprising the photopeak for each line correspond to complete energy conversion of the gamma ray. Because of the small size of the germanium detector employed in the present measurements, other features appeared prominently in the measured pulse-height spectra arising from incomplete energy conversion of the gamma ray. Two such features that occur for gamma rays with sufficient energy to pair produce are the single- and double-escape peaks, located 0.51 and 1.02 MeV below the photopeak. These features are quite evident in Fig. 6 in which they are labelled FE and SE, respectively.

For the gamma-ray energies of interest in the present experiment, Compton scattering also is an important energy-loss mechanism. The Compton continuum is produced by gamma rays of all energies and is most noticeable as a shoulder located typically 200 to 250 keV below the photopeak. Figure 7 shows a pulse-height spectrum resulting from a monoenergetic (0.662 MeV) flux of gamma rays incident on the detector employed in the present work. The resolution is much better for this spectrum than for the spectra measured for determination of cross sections due to re-annealing of the crystal subsequent to the other measurements. The photopeak is the sharp feature near channel 660, and the events in the channels below it comprise the Compton continuum. The Compton edge occurs at a pulse-height corresponding to the energy lost to an electron by a gamma ray that scatters through 180 degrees and suffers no further interaction in the crystal. This edge, as well as the Compton continuum, provide a significant source of background in this experiment.

Although subject to the same interaction mechanisms, a high-energy (greater than about 10 MeV) beam of monochromatic gamma rays incident on the HPGe detector does not produce the same prominent features that are produced by the low-energy gamma rays. Two typical pulse-height spectra measured for this work are shown in Figs. 3(c) and 3(d). As is seen in Fig. 3(d), the 15.10-MeV gamma rays produced in the reaction $^{12}C(p,p'\gamma_{15.10})^{12}C$ result in a single, broad feature (greater than 1 MeV FWHM) in the pulse-height spectrum. The photopeak, the escape peaks, and the Compton edge are no longer distinguishable, and the position of the maximum in the detector response is shifted downward in energy from 15.10 MeV. These effects are caused primarily by the high probability that an energetic electron, produced by the interaction of a high-energy gamma ray, will escape from the crystal.

Figure 6 shows a detailed portion of a pulse-height spectrum in the 4- to 6-MeV energy range. This pulse-height spectrum represents the HPGe response to the gamma-ray flux at 70 degrees to the 40-MeV proton beam. The long-lived nuclear states $^{16}O^*(6.130)$, $^{15}O^*(5.241)$, $^{15}N^*(5.270)$, and $^{14}N^*(5.106)$ produce relatively

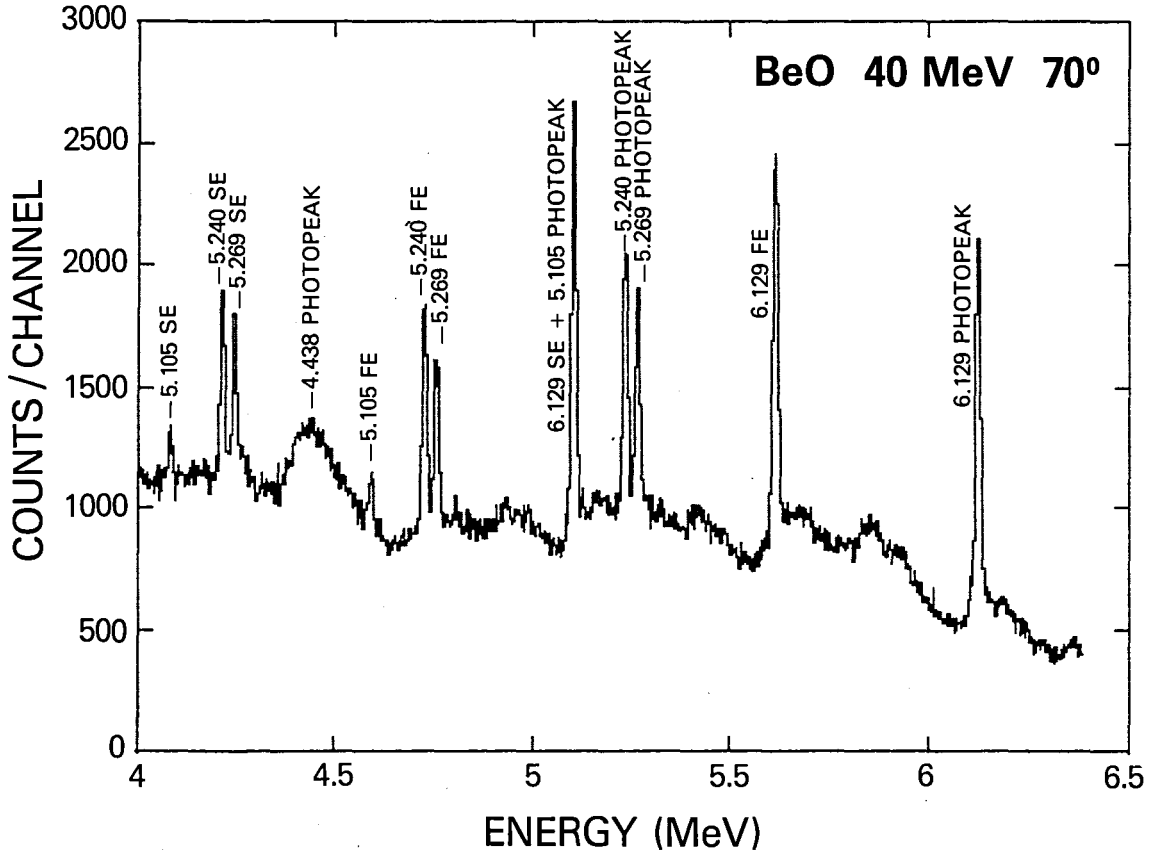

Figure 6. A portion of a pulse-height spectrum for 40-MeV protons incident on the BeO target measured at 70 degrees to the proton beam. Each point is one raw pulse-height channel. This portion corresponds to the energy range from approximately 4.0 to 6.4 MeV and includes the narrow gamma-ray lines at 6.129, 5.269, and 5.240 MeV along with their first- and second-escape peaks. Also evident are the narrow 5.105-MeV first- and second-escape peaks (the photopeak is coincident with the second-escape peak of the 6.129-MeV line) and the broad 4.438-MeV photopeak from ^{12}C. Note the irregularity of the background, indicating unresolved gamma-ray lines and Compton edges.

narrow features in the measured gamma-ray pulse-height spectra. These excited nuclei have time to come to rest in the solid targets used in this experiment and, consequently, the corresponding gamma-ray lines are relatively narrow. The widths of these lines correspond to the resolution of the detector at these energies. The photopeak and escape peaks for the 6.129-, 5.271-, and 5.240-MeV gamma-ray lines stand out in Fig. 6 and are marked. The 5.105-MeV photopeak from ^{14}N is only 2 keV from the second-escape peak associated with the 6.129-MeV line and is not resolved, but the ^{14}N escape peaks are present and are marked.

Most of the excited nuclear states produced in the present experiment have lifetimes shorter than a picosecond. These excited nuclei do not come to rest in the targets before de-exciting, and, consequently, the corresponding gamma-ray lines are not monochromatic; they exhibit significant Doppler broadening and thus appear broadened in the pulse-height spectra. This Doppler broadening, as well as any structure such as the double peaks of the ^{12}C 4.438-MeV line, are also reproduced in the escape peaks and the Compton edge.

A number of broad features are evident in Fig. 6. The largest of these is the 4.438-MeV line from the $^{16}O(p,x\,\gamma_{4.438})^{12}C$ reaction. Some of the broad features in the spectrum can be attributed to unresolved

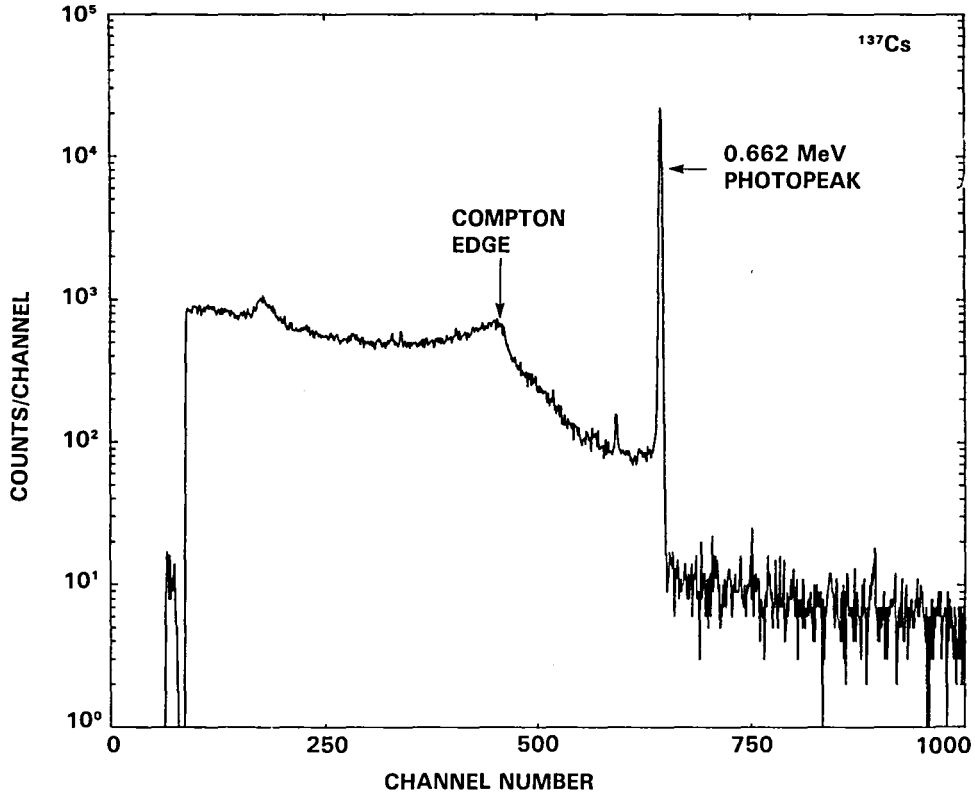

Figure 7. Pulse-height spectrum for monoenergetic, 0.662-MeV gamma rays incident on the HPGe detector employed in the present cross section measurements. This line arises from the decay of ^{137}Cs to the 0.662-MeV level of ^{137}Ba. At the time this spectrum was measured, the detector had been re-annealed so that the resolution was much better than it had been at the time the cross section measurements were obtained. The energy scale is linear and corresponds to approximately 1 keV per channel. The photopeak occurs near channel 660, while the Compton edge occurs near channel 480.

Doppler-broadened lines, escape peaks from such lines, and broad Compton edges from all lines. In future experiments, it might be possible to suppress greatly such escape peaks and Compton edges with the use of active anticoincidence shields surrounding a high-resolution detector.

IV.A.2. Areas using a template from the data

Gamma rays from the decay of the 15.11-MeV level of ^{12}C and incident on the detector produced a single, broad, highly non-Gaussian feature in the measured pulse-height spectra. To determine the area of this feature, a template had to be determined from the data. The pulse-height spectrum from the measurement with the highest signal-to-noise ratio in the energy range from about 12.26 MeV to 15.50 MeV was selected for this purpose.

A linear background was determined from the spectral region above 15.50 MeV in the same pulse-height spectrum. An empirical peak shape was constructed from the raw pulse-height spectrum by subtracting the extrapolation of the linear background. This peak shape was then summed into bins with twenty pulse-height channels each (about 50 keV) and was smoothed, giving a total of about sixty bins in the final line-shape template. A background template was constructed by integrating the linear fit over the same twenty-channel

bins. Both templates were normalized to unit area. The 15.10-MeV gamma-ray line area was then determined at each energy and angle by performing a least-squares fit of the measured data to the sum of the two templates, each multiplied by a variable amplitude.

IV.A.3. Areas using theoretical templates

The photopeaks and escape peaks due to the 4.438-MeV gamma-ray line from the BeO target exhibit significant Doppler broadening (see Fig. 6 and Sec. III.B). There are a number of significant factors that affect the determination of the corresponding gamma-ray line areas. Figure 6 shows that the first escape peak from the 5.105-MeV line, at 4.594 MeV, is considerably narrower than the 4.438-MeV photopeak and is superposed on its high-energy tail. Escape peaks from the resolved 5.240- and 5.269-MeV narrow lines and the unresolved 5.182- and 5.300-MeV Doppler broadened lines, all from ^{15}O and ^{15}N, bracket and partially overlap the 4.438-MeV photopeak. As a result of all these effects, an accurate knowledge of the 4.438-MeV line shape is required to determine the gamma-ray line areas from the measured pulse-height spectra.

The model for the $^{16}O(p,x\ \gamma_{4.438})^{12}C$ reaction outlined in Sec. III.B was derived in order to calculate the expected shape of the gamma-ray line. To compute this line shape at the proton energies used in this experiment (40, 65, and 85 MeV), it is necessary to know a number of parameters. One of these is the angular dependence of the differential proton scattering cross section at each energy. Differential cross sections are available in the literature at $E_p = 45$ MeV,[16] but only for the giant dipole region of ^{16}O (an excitation energy range from 21.5 MeV to 27 MeV). For the present work, the angular dependence of this cross section at 45 MeV has been adopted for 40-MeV protons and has been assumed to be the same for all levels.

In addition to the differential proton scattering cross section, the excitation function for states which are strongly excited in the reaction $^{16}O(p,p')^{16}O^*$, as well as the probability of alpha decay of these states to $^{12}C^*(4.439)$, must also be known for 40-MeV protons. Below an ^{16}O excitation energy of 16 MeV, the 45-MeV (p,p') spectrum consists of a series of isolated peaks for which the associated widths for decay into $^{12}C^*(4.439) + \alpha_1$ are known.[18–20,22] In Table II the values of $\Gamma_{\alpha 1}(E_N)/\Gamma_{tot}(E_N)$ for the peaks as well as the products with $\sigma(40°,E_N)$ are given; the width ratios are derived from Table I. For the peaks at 13.02 and 15.50 MeV, each of which consists of at least a pair of unresolved states, the "effective" ratio is given.

For excitation energies greater than 16.0 MeV the spectrum consists of definite peaks above a constantly increasing background. This background can be attributed to (p,2p) and (p,pn) quasi-free processes which do not contribute to the production of $^{12}C^*(4.439)$ gamma rays. The authors of Ref. 16 have used a straight line background which is non-zero well below the thresholds for $^{15}N + p$ and $^{15}O + n$ at 12.13 and 15.67 MeV, respectively. For this reason, a more realistic form of the background was required.

In the spectrum of the scattered protons the quasifree peak is both shifted to higher energy transfer and broadened compared to the narrow elastic peak observed in proton scattering from a free nucleon. A 45-MeV proton scattering from a free nucleon through an angle of 40 degrees transfers 18.6 MeV to the struck nucleon. Adding to this the 12.1-MeV binding energy, the total energy transferred to a proton in a quasi-free scattering is approximately 31 MeV. There is the added complication that the ejected proton is indistinguishable from the incident proton and its energy of $31 - 12 = 19$ MeV, if attributed to a projectile proton, indicates an excitation in ^{16}O of about 26 MeV. Therefore the form of the background cross section which was substituted is

$$\sigma_{bg} = 1.36[e^{-(31-E_N)^2/\xi^2} + 0.25e^{-(26-E_N)^2/\xi^2}], \tag{26}$$

Table II. Contributions of each energy region of the $^{16}O(p,p')^{16}O^*$ spectrum to the $^{16}O(p,x\ \gamma_{4.438})^{12}C$ reaction. Values of $\Gamma_{\alpha 1}(E_N)/\Gamma_{tot}(E_N)$ are derived from Table I, and the cross sections at 40 degrees were taken from Ref. 16. Where pairs of states were unresolved the shape of the experimental peak was fit with the sum of two Breit-Wigner resonant shapes using the known total and partial width. The total cross section estimate was obtained by using the differential cross section averaged over the giant dipole region displayed in Fig. 3 of Ref. 16.

E_N (MeV)	$\Gamma_{\alpha 1}/\Gamma_{tot}$	$\frac{\Gamma_{\alpha 1}}{\Gamma_{tot}}\sigma(40°,E_N)$ (mb/sr)
12.53	1.0	0.26
13.02, 13.26	0.12	0.14
13.97	0.42	0.25
15.27, 15.50	0.43	0.88
16–18	0.33	0.60
18–20	0.33	0.90
20–22	0.33	0.61
22–24	0.33	0.54
24–26	0.33	0.36
26–28	0.33	0.11

where σ is in units of mb/(sr MeV) and $\mathscr{E} = 7.2$ MeV. The remaining two parameters in the model for the background cross section have been chosen to give a reasonable fit to the cross section above $E_N = 27$ MeV, taking into account the fact that the ratio σ_{pn} to σ_{pp} is approximately three at the energy of interest.

Because the peaks above $E_N = 16$ MeV are overlapping in the (p,p') spectrum, it was necessary to divide the spectrum into 2-MeV wide bins centered at 17, 19, 21, 23, 25, and 27 MeV. While the ratio $\Gamma_{\alpha 1}/\Gamma_{tot}$ averages 0.42 below 16 MeV, it should become smaller above the opening of the $^{15}O + n$ channel at 15.67 MeV. Therefore, the central values of $\sigma(40°,E_N)\ \Gamma_{\alpha 1}(E_N)/\Gamma_{tot}(E_N)$ reported in Table II are derived by assuming that $\Gamma_{\alpha 1}/\Gamma_{tot} = \frac{1}{3}$.

Using the above results, the gamma-ray line profiles at five angles for 40-MeV protons incident on BeO were computed. Because the resolution of the HPGe detector is much smaller than the width of these profiles, broadening due to the finite resolution of the detector on the shape of the templates in the fits is negligible. The templates were normalized to unit area and were fit to the photopeaks in the measured pulse-height spectra, along with an underlying quadratic background, to determine the desired gamma-ray line areas. The fit of the template to the data at 70° is shown in Fig. 8, in which the quadratic background has been removed. The "gap" in the spectrum at the right side corresponds to the location of the first-escape peak of the 5.105-MeV gamma-ray line from ^{14}N; the portion of the pulse-height spectrum in this gap was excluded during the fits.

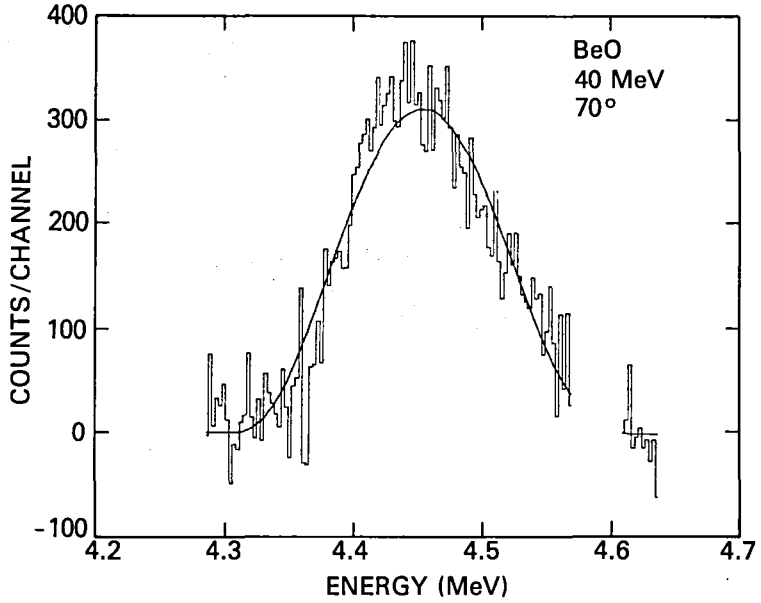

Figure 8. Residuals (background has been subtracted) for a portion of the pulse-height spectrum obtained with 40-MeV protons incident on the BeO target measured at 70 degrees to the proton beam. Each point is one raw pulse-height channel. This portion corresponds to the energy range from approximately 4.3 to 4.65 MeV. Included is the broad gamma-ray line at 4.438 MeV from the reaction $^{16}O(p,x\ \gamma_{4.438})^{12}C$. Also shown as a solid line is the fit to the background and line complex using the template computed as discussed in Sec. IV.A.3.

IV.A.4. Areas using Gaussian templates

The remaining peaks in the measured pulse-height spectra have shapes that are essentially Gaussian. The computer program HYPERMET[26] provides an automated technique for the determination of the areas of such peaks. HYPERMET requires that certain fitting parameters be adjusted for each detector. The optimum values for most parameters had been determined from previous analysis of monoenergetic gamma-ray lines. For this work, all that was required for HYPERMET to analyze a spectral feature, besides the pulse-height spectrum, is the specification of a range of pulse-height channels and an estimate of the expected peak width within that range.

HYPERMET[26] begins the analysis by performing a peak search by application of a square transform. The positions of large, positive values in the transform correspond to peaks in the spectrum. Each peak is modelled with a peak-shape function consisting of four terms: a term corresponding to discrete-energy gamma rays from an ideal source; a skew term expressed as a decaying exponential on the low-energy side of the peak, compensating somewhat for incomplete charge collection and pile-up; a low-energy tail identical in form to the skew term but with a smaller amplitude and a larger slope, possibly due to surface effects; and, if a peak is designated to be an escape peak, a step in the background continuum due to Compton scattering or due to summing of multiple-photon events. Each of these terms is folded with a Gaussian to simulate normally distributed statistical and electronic noise inherent to the detection process. Underlying the peak(s) in the fit is a background which is represented by a function that is quadratic in pulse-height channels.

An iterative least-squares fit is performed over the specified range of channels to determine the peak-shape and background parameters that minimize the reduced chi-square function. The initial fit is performed

with peaks at the positions determined from the square-transform application described above. This fit is accepted if chi-square is less than its expected value plus an amount corresponding to a specified number of standard deviations. If it exceeds this value, the residuals are searched for additional peaks. A peak at the position of the largest residual is added to the fitting function and the fit is repeated. This procedure continues until an acceptable chi-squared is obtained, until no additional peaks are found, or until a specified maximum number of tries is reached. The number of pulse-height events in each peak is obtained from the integral of the first two peak-shape terms and is the desired gamma-ray line area. The other peak-shape terms are considered to contribute to the background.

HYPERMET has been employed to determine the area of all significant spectral features from about 2.0 to 4.8 MeV for p + ^{12}C and from about 2.0 to 6.3 MeV for p + ^{16}O. The photopeak areas derived thusly were deemed sufficiently reliable for the determination of the gamma-ray production cross sections in these energy ranges *except* for the 5.105-MeV line from ^{14}N and the 4.438-MeV line from both targets. The 4.438-MeV line from the oxygen target is discussed in Sec. IV.A.3. Because the 5.105-MeV photopeak cannot be resolved from the 6.129-MeV second-escape peak, the first-escape peak areas were selected for use in the determination of the desired cross sections. The corresponding detector efficiency is discussed in Sec. IV.A.5.

HYPERMET was employed in the initial determination of the 4.438-MeV gamma-ray line areas of the photopeaks resulting from the reaction $^{12}C(p,p'\gamma_{4.438})^{12}C$. Difficulties were encountered, however, because HYPERMET was designed to determine areas from pulse-height spectra for lines that are narrow relative to changes in the background such as Compton edges, while the intrinsic line profile from the reaction $^{12}C(p,p'\gamma_{4.438})^{12}C$ is so broad, as discussed in Sec. III.A, that it overlies numerous spectral features which comprise its background. Consequently, an additional technique was developed to determine areas for this line.

Ideally, the expected line profile would be computed from the formalism in Sec. III.A and the resulting shapes would be used as templates in fits to the data. To do this, however, would require a knowledge of the relative population of the five magnetic sublevels of this excited state [$J^\pi = 2^+$; see Eq. (4)]. Because no such information was available for this experiment, the line shape could not be computed analytically.

As an alternative, a line shape was constructed using as many as three Gaussians. Reduced pulse-height spectra were constructed by subtracting the best-fit quadratic backgrounds derived by HYPERMET from the raw pulse-height spectra. The 4.438-MeV photopeaks in the reduced spectra were fit using a least-square technique.[27] In the resulting fits, one or two Gaussians generally sufficed to simulate the reduced line profile. A third Gaussian was sometimes required to compensate either for a possible contribution from the ^{11}B line at 4.444 MeV (but see Sec. V.A.4) or the highly non-Gaussian line profiles arising from the coherent Doppler effect (see Sec. III.A). A second set of areas for this line were derived using this technique for all ^{12}C target pulse-height spectra.

For each pulse-height spectrum, the two values of chi-squared from the two techniques were compared. The 4.438-MeV gamma-ray line area determined by the better fitting technique was selected as the best estimate of the area of the photopeak. This set of areas, about half from HYPERMET and half from the multiple-Gaussian technique, were used to determine gamma-ray production cross sections as described in Sec. IV.B.

All of the fitting techniques above provided not only a measure of the gamma-ray line areas for the selected pulse-height features but also the corresponding statistical uncertainties. In a few cases, for the 6.129-MeV line only, some of the derived uncertainties in the areas were determined to be much larger than could be attributed to counting statistics alone. For those few cases, more reasonable estimates of the uncertainties were computed from consideration of the raw spectra and from the results of the HYPERMET fit. The more

reasonable values for the uncertainties are used in Sec. IV.B in which determination of the differential gamma-ray production cross sections, and thence the total cross sections from the gamma-ray line areas, are presented.

IV.A.5. Detector efficiencies

Seltzer[9] has estimated absolute detector efficiencies for gamma rays with energies from 2 to 20 MeV incident on the detector employed in the present measurements. His results have been used to compute the detector efficiency for converting incident gamma rays to an event in the photopeak for the gamma-ray lines of interest in this work, except for the 5.105-MeV and 15.10-MeV lines. Seltzer's computations provided an estimate of the absolute detector efficiency for 15.10-MeV gamma rays only for the integral energy range from 14.08 MeV to 15.10 MeV. Because the fits described in Sec. IV.A.2 determined the line areas in the feature from 12.26 MeV to 15.10 MeV, the detector efficiency was normalized to this energy range by dividing it by the fraction of the (normalized) gamma-ray line template from 14.08 MeV to 15.10 MeV.

Seltzer also employed his Monte Carlo technique to compute an estimate of the detector efficiency for first-escape peaks. Analysis of the photopeaks and first-escape peaks of the strong, narrow lines at 6.129, 5.269, and 5.240 MeV indicated a systematic difference (about 10%) between the cross sections derived using first-escape areas and efficiencies and those derived using the photopeak areas and efficiencies. This 10% correction has been applied to the measured 5.105-MeV gamma-ray production cross sections.

IV.B. Determination of gamma-ray production cross sections from gamma-ray line areas

The techniques discussed in Sec. IV.A have been used to determine the gamma-ray line areas of selected features in the measured pulse-height spectra. A differential gamma-ray production cross section, in mb/sr, proportional to the corresponding area, is determined according to the following equation:

$$\frac{d\sigma}{d\Omega}(E_\gamma,T,E_p,\theta) = \exp\left[\frac{\mu_{Be}(E_\gamma)x_0(Be)}{\sin\theta}\right]\frac{C(E_\gamma,T,E_p,\theta)}{F(T,E_p,\theta)} \times \exp[\mu_{Al}(E_\gamma)x_0(Al) + \mu_{Ge}(E_\gamma)x_0(Ge)] \times \frac{1}{\epsilon(E_\gamma)}\frac{A(T)}{t(T)}\frac{10^{27}}{\Omega}\frac{e}{kN_{AVOG}}, \quad (27)$$

where $\mu_{element}(E_\gamma)$ is the mass absorption coefficient for the indicated absorbing material in cm^2/g; x_o(element) is the thickness of the absorbing material in g/cm^2; $C(E_\gamma,T,E_p,\theta)$ is the gamma-ray line area for the selected feature in the pulse-height spectrum; $F(T,E_p,\theta)$ is the charge accumulated by the Faraday cup, in units of 10^{-11} Coulombs; $\epsilon(E_\gamma)$ is the intrinsic detector efficiency for converting photons of energy E_γ into events in the selected spectral feature; A(T) is the molecular weight of the BeO or CH_2 target in g/mole; t(T) is the target thickness in g/cm^2; Ω is the solid angle subtended by the detector; 10^{27} converts the cross section from cm^2/sr to mb/sr; e is the charge of a proton in Coulombs; k is the factor for converting F to Coulombs; and N_{AVOG} is Avogadros's number, in mol^{-1}. The independent variables of which the differential cross section is a function are E_γ, the energy of the gamma-ray; T, the target (CH_2 or BeO); E_p, the energy of the incident proton; and θ, the angle of observation with respect to the incident beam direction.

To determine the total gamma-ray production cross section, the differential cross section could, in principle, be integrated over all solid angle. Because only five independent determinations of the differential

cross section for each E_γ, T, and E_p were made in this work, numeric integration would not be reliable. It is fortunate that the physics of the problem shows that the angular distribution of gamma rays is expected to be of the form

$$\frac{d\sigma}{d\Omega}(E_\gamma,T,E_p,\theta) = \sum_{l=0;\,l\,\text{even}}^{L} a_l(E_\gamma,T,E_p)P_l(\cos\theta), \tag{28}$$

where $P_l(\cos\theta)$ are Legendre polynomials and the a_l's are parameters to be determined from the data. The sum is performed over even values of l from zero to L, where L is the lesser of i) twice the multipolarity of the gamma ray and ii) twice the spin of the decaying nuclear state.

For the gamma-ray lines of interest in the present work, the largest value of L is 6, for the ^{16}O 6.129-MeV line (a 3^- to 0^+ transition). In all cases, there are thus at most four terms in the Legendre polynomial expansion of the angular distribution. The five angular measurements reported here allowed all coefficients to be determined. To arrive at a total cross section, Eq. (28) is integrated analytically to obtain

$$\sigma_{TOT}(E_\gamma,T,E_p) = 4\pi a_o(E_\gamma,T,E_p). \tag{29}$$

All of the angular dependence of the differential cross section is contained in three terms in Eq. (27). The terms $C(E_\gamma,T,E_p,\theta)$ and $F(T,E_p,\theta)$ are discussed above. The angular-dependent exponential term corrects the measured area for the gamma-ray absorption by the beryllium block employed to shield the detector from scattered protons and charged reaction products (see Sec. II and Fig. 1). The numerical value of this correction ranges from 1.2 to 2.4, with the maximum being at the largest angle and the smallest gamma-ray energy. In order to determine the coefficients of the Legendre polynomials as accurately as possible, the differential cross section was expressed as

$$\frac{d\sigma}{d\Omega}(E_\gamma,T,E_p,\theta) = \Theta(E_\gamma,T,E_p,\theta)/[\eta(t)q(E_\gamma)\Omega\epsilon(E_\gamma)], \tag{30}$$

where

$$\Theta(E_\gamma,T,E_p,\theta) = \exp\left[\frac{\mu_{Be}(E_\gamma)x_o(Be)}{\sin\theta}\right]\frac{C(E_\gamma,T,E_p,\theta)}{N_p(T,E_p,\theta)}, \tag{31}$$

$$N_p(T,E_p,\theta) = kF(T,E_p,\theta)/e, \tag{32}$$

$$\eta(T) = \frac{t(T)}{A(T)}\frac{N_{AVOG}}{10^{27}}, \tag{33}$$

and

$$q(E_\gamma) = \exp\{-[\mu_{Al}(E_\gamma)x_o(Al) + \mu_{Ge}(E_\gamma)x_o(Ge)]\}. \tag{34}$$

Because all of the angular dependence of the cross section in Eq. (30) is now contained in the function $\Theta(E_\gamma,T,E_p,\theta)$, the angular fits could be performed with respect to Θ instead of with respect to the differential cross section:

$$\Theta(E_\gamma,T,E_p,\theta) = \sum_{l=0;\,l\,\text{even}}^{L} b_l(E_\gamma,T,E_p)P_l(\cos\theta). \tag{35}$$

This allowed the angular dependence of the cross section to be determined while including only uncertainties in the counting statistics. When the Legendre polynomial coefficients, b_l, are computed this way, the total cross section is given by

$$\sigma_{TOT}(E_\gamma,T,E_p) = 4\pi b_o(E_\gamma,T,E_p)/[\eta(T)q(E_\gamma)\Omega\epsilon(E_\gamma)], \quad (36)$$

in analogy to Eq. (29). Figure 9 shows the experimental values of $k\Theta/e$ plotted as a function of observation angle for selected gamma-ray lines. Also shown are the Legendre-polynomial fits for these five lines.

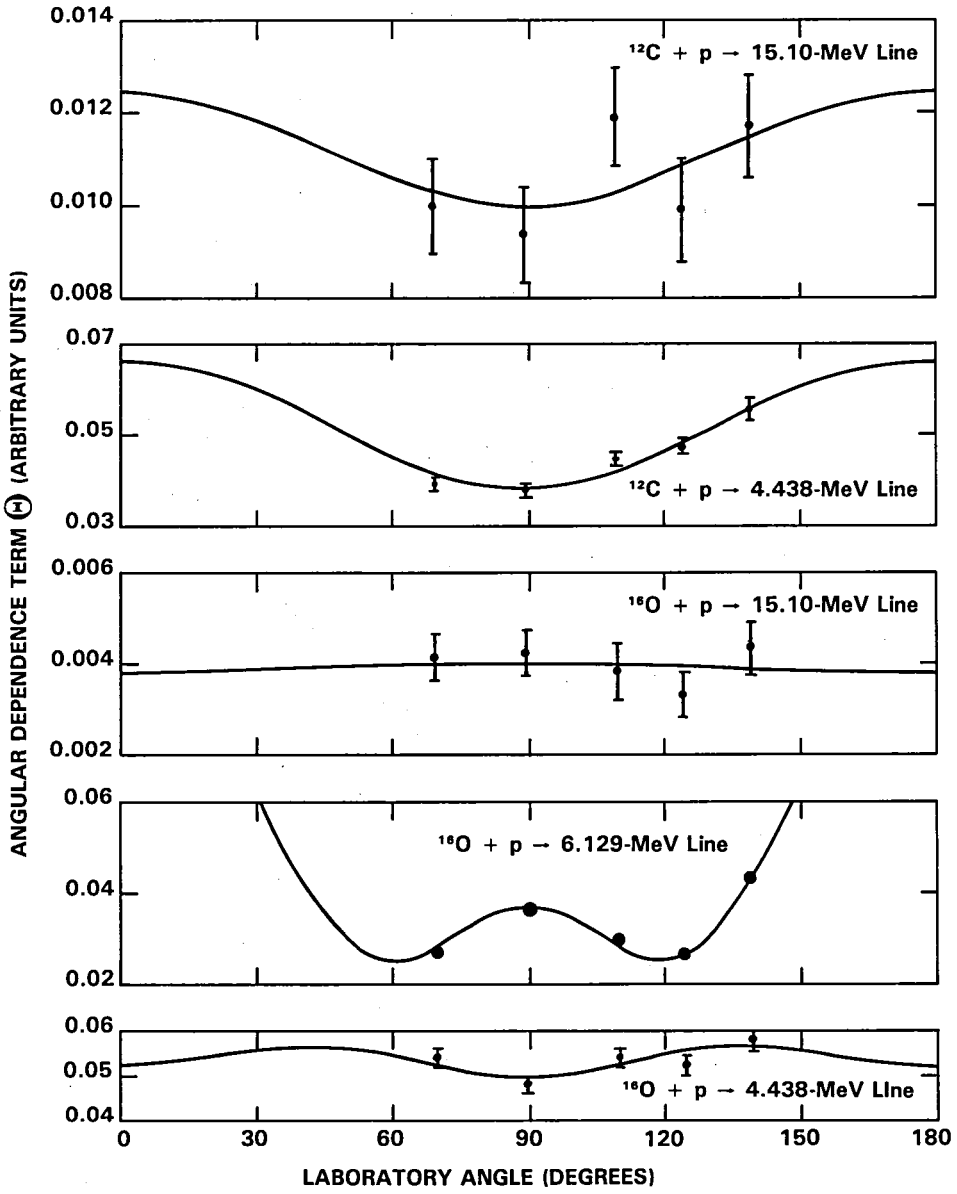

Figure 9. Angular dependence of selected differential gamma-ray production cross sections. The circles represent the present measurements of the angular-dependence term, $\Theta(E_\gamma,T,E_p,\theta)$, times k/e, for the five observation angles. The solid curves show the results of a least-squares fit of the data to a sum of Legendre polynomials.

There are two small corrections to the measured values of Θ that have been neglected when fitting to the Legendre-polynomial series of Eq. (35). The first, the variation of the Legendre polynomials over the gamma-ray detector area, has been determined to cause less than a one percent difference in the total cross section. The second, due to the transformation from laboratory to center-of-momentum values of the gamma-ray emission angles, has been determined to be less than 2.5 percent for the case of 85-MeV protons incident on ^{12}C.

The desired total gamma-ray production cross sections may be determined in a straightforward manner. For a particular gamma-ray line, the gamma-ray areas from Sec. IV.A are used to determine $\Theta(E_\gamma,T,E_p,\theta)$. For a fixed T and E_p, these values are fit to the angular distribution of Eq. (35). The total gamma-ray production cross section is then computed using the first coefficient from the fit according to Eq. (36).

For some of the parameters used to calculate cross sections, there are systematic uncertainties which could not be quantitatively estimated *a priori*. The detector efficiency, $\epsilon(E_\gamma)$, and the solid angle subtended by the detector, Ω, very likely include the largest systematic uncertainties. The detector efficiencies were computed with a Monte Carlo technique by Seltzer[9] for a parallel beam of gamma rays incident on an ideal 58 mm in diameter by 46 mm cylindrical detector. The detector employed in this experiment had sustained neutron damage prior to use. Not only did this reduce the resolution of the detector, but it reduced the active volume of the detector. An additional factor was the existence of a finger for charge collection that reduced the physical volume of the detector by about one percent, and the effective volume for complete conversion to pulse height by an even larger factor. Corrections for both of these factors would reduce the true photopeak efficiencies and raise the cross sections, however, a quantitative description is unavailable.

The value of the detector efficiency computed by Seltzer[9] is also quite sensitive to the parallel beam assumption, which requires both that the beam be strictly parallel and that the sides of the detector be oriented parallel to the beam. The beam at the detector (only 1.8 m from the target) could not be strictly parallel, and the cylindrical detector was not precisely aligned so that its symmetry axis would pass throught the center of the target. In addition, the solid angle depends somewhat on the positioning of the detector, and there are additional ambiguities in the positioning of the detector that cannot be resolved. Because these were known to be potential systematic uncertainties at the time this experiment was performed, it was decided in advance to normalize the measured cross sections [as given by Eq. (36)] to published values that were believed to be well determined.

These normalized cross sections are determined as follows. The ratio of the well-determined cross section from the literature to the corresponding measured cross section determined from Eq. (30) or Eq. (36) is computed. The remaining cross sections are normalized by multiplying by this value. If the components of the normalized cross sections are visualized as being expressed in terms of Eq. (30) or Eq. (36), systematic uncertainties due to the solid angle are seen to cancel immediately. While the absolute values of the detector efficiency may also contain systematic uncertainties, the ratio of two photopeak efficiencies is believed to be correct. Additional systematic uncertainties exist with the 5.105-MeV and 15.10-MeV efficiencies which are not photopeak efficiencies.

The normalization factors have been determined from well-determined cross sections. The total excitation cross section for the reaction $^{12}C(p,p')^{12}C^*(4.439)$ has been estimated from the differential cross section of Stovall and Hintz[28] to be 42.9 $\pm$ 1.0 mb for 39.8-MeV protons. With a gamma-ray branching ratio of 1.0 and no significant contribution from higher-lying levels, this is equal to the 4.438-MeV gamma-ray production cross section. The normalization factor is then 1.3 $\pm$ 0.2.

For confirmation, the gamma-ray production cross sections for the reaction $^{16}O(p,p'\gamma_{6.129})^{16}O$ have been estimated from the excitation cross sections. Austin *et al.*[29] present measurements of the total excitation cross

sections for the reactions $^{16}O(p,p')^{16}O^*$(6.130 and 8.872) for 39.7-MeV protons. When these are combined with an estimate of the 11.080-MeV excitation cross section and the known branching ratios for decay through the 6.130-MeV state, the 6.129-MeV gamma-ray production cross section is estimated to be 34.8 ± 2.0 mb for 40-MeV protons. The normalization factor for this cross section is found to be 1.3 ± 0.2, the same as for the 4.438-MeV ^{12}C cross section. This is important as it indicates that the major sources of systematic errors have probably been eliminated from the normalized cross sections, except perhaps for the 15.10-MeV line discussed below.

A different normalization factor is required for the 15.10-MeV gamma-ray production cross sections. The only gamma-ray production cross section reported for the reaction $^{12}C(p,p'\gamma_{15.10})^{12}C$ for 40-MeV protons was a measurement of the differential cross section by Measday *et al.*[30] They reported a value of 0.12 ± 0.02 mb/sr at 90 degrees to the proton beam. Results from the present experiment indicate that the 15.10-MeV gamma-ray emission is significantly anisotropic for this reaction (See Fig. 9). For this reason, the normalization factor must be computed from the present differential cross section measurement for the above reaction. This value is 0.072 ± 0.011 mb/sr, giving the normalization factor used for all 15.10-MeV cross sections of 1.7 ± 0.4.

V. RESULTS AND CONCLUSIONS

V.A. Gamma-ray production cross sections

The gamma-ray production cross sections determined in this work are presented in Table III. The first column gives the energy of the observed gamma-ray line and the second column gives the target material. The next three columns indicate the most probable excited nucleus, initial state, and final state involved in each transition.

Two sets of cross sections are presented in Table III. These two sets of cross sections are discussed in Sec. IV.B. Briefly, the first set, labelled "as measured," is the set of cross sections determined according to the formalism of Eq. (36) and uses the detector efficiencies of Seltzer.[9] When these values are compared to values already reported in the literature (see this and the following sections), the results obtained in the present work are found to be systematically lower. This is not a totally unexpected result, as there are known to be systematic effects that cannot be estimated quantitatively with the desired precision. The second set of cross sections, labelled "normalized," have been normalized to published values that are believed to be well determined. Unless specifically noted, the discussion of the results in the following sections will refer to these normalized values.

V.A.1. $^{12}C(p,p'\gamma_{15.10})^{12}C$

Measurements of the 15.10-MeV differential gamma-ray production cross section from p + ^{12}C normalized to the reported measurements of Measday *et al.*[30] for 40-MeV protons are presented in Table III. In Fig. 10, the upper three filled circles represent the present measurements. The shaded region represents the confidence interval of the differential cross sections measured by Measday *et al.* for 16.7- to 48.5-MeV protons[30] and Warburton and Funsten for 14- to 20-MeV protons.[31] These measurements were obtained only at a laboratory scattering angle of 90° and, for purposes of comparison with the total gamma-ray production cross sections, were multiplied by 4π steradians. This approximation neglects the fact that the gamma rays are not necessarily emitted isotropically in the laboratory frame. Angular fits to the present data indicate that gamma-ray emission is significantly anisotropic for protons in the 40–85 MeV range. Because the gamma-ray emission is anisotropic, the present total cross section is not centered on the shaded region.

Table III. Table of total gamma-ray production cross sections for protons incident on the indicated target and producing the indicated gamma-ray line. Most probable transition for production of the observed gamma-ray line is given. The first column gives the energy of the gamma-ray line and the second column gives the target material. The next three columns indicate the most probable excited nuclei, initial states, and final states involved in the transitions. The first set of cross sections, labelled "as measured," are the cross sections determined according to the formalism of Eq. (36). The second set, labelled "normalized," have been normalized to published cross sections that are believed to be well determined. The numbers in parentheses are the uncertainties in the last two (or three) digits of the indicated cross section.

E_γ (MeV)	Target	Excited nucleus; spin and parity of initial and final states			Total gamma-ray production cross section (millibarns)					
					As Measured			Normalized		
					40 MeV	65 MeV	85 MeV	40 MeV	65 MeV	85 MeV
15.10	BeO	^{12}C	1^+	0^+	0.237(29)	0.105(14)	0.112(19)	0.402(107)	0.179(49)	0.190(55)
15.10	CH_2	^{12}C	1^+	0^+	1.044(149)	0.657(93)	0.486(72)	1.77(49)[a]	1.12(31)	0.83(23)
4.438	BeO	^{12}C	2^+	0^+	23.9(27)	b	b	31.1(59)	b	b
4.438	CH_2	^{12}C	2^+	0^+	34.3(48)	13.1(19)	8.8(13)	44.5(93)[a]	17.0(36)	11.5(25)
6.129	BeO	^{16}O	3^-	0^+	27.0(33)	10.5(13)	9.5(13)	35.1(69)[a]	13.6(27)	12.3(25)
5.269	BeO	^{15}N	$5/2^+$	$1/2^-$	8.82(101)	4.27(49)	3.23(39)	11.47(220)	5.55(107)	4.20(82)
5.240	BeO	^{15}O	$5/2^+$	$1/2^-$	12.45(141)	6.86(77)	5.43(63)	16.2(31)	8.9(17)	7.1(14)
5.105	BeO	^{14}N	2^-	1^+	4.38(91)	3.79(65)	2.32(38)	5.70(148)	4.92(114)	3.02(68)
2.793	BeO	^{14}N	2^-	0^+	0.543(75)	0.628(78)	0.487(70)	0.71(15)	0.82(16)	0.63(13)
2.741	BeO	^{16}O	2^-	3^-	2.74(30)	1.75(20)	1.37(17)	3.56(67)	2.27(44)	1.78(35)
2.313	BeO	^{14}N	0^+	1^+	8.36(88)	6.99(74)	5.90(63)	10.9(20)	9.1(17)	7.7(14)
2.154 + 2.124	CH_2	^{10}B ^{11}B	1^+ $1/2^-$	3^+ $3/2^-$	4.70(65)	3.74(54)	3.72(53)	6.11(127)	4.86(103)	4.83(102)
2.000	CH_2	^{11}C	$1/2^-$	$3/2^-$	9.50(128)	7.52(102)	6.96(95)	12.4(25)	9.8(20)	9.1(19)

[a] These values are normalized to well-determined cross sections; see Sec. IV.B.

[b] No cross sections since templates could only be computed for 40-MeV protons.

The open points in Fig. 10 represent reported measurements of the 15.11-MeV excitation cross section for the reaction $^{12}C(p,p')^{12}C^*(15.11)$, multiplied by the 15.10-MeV gamma-ray branching ratio of 0.9. These points are determined from the results of Warburton and Funsten for 19.5-MeV protons,[31] Scott, Fisher, and Chant for 20.5- to 30.3-MeV protons,[32] Geramb *et al.* for 22.5- to 45-MeV protons,[33] Dickens, Haner, and Waddell for 31.1-MeV protons,[34] Petersen *et al.* for 46-MeV protons,[35] Amos *et al.* for 62-MeV protons,[36] and Hasselgren *et al.* for 185-MeV protons.[37]

In 1979, Crannell, Crannell, and Ramaty[4] summarized the 15.10-MeV gamma-ray production cross sections reported in the literature as well as the corresponding excitation cross sections by inelastic proton

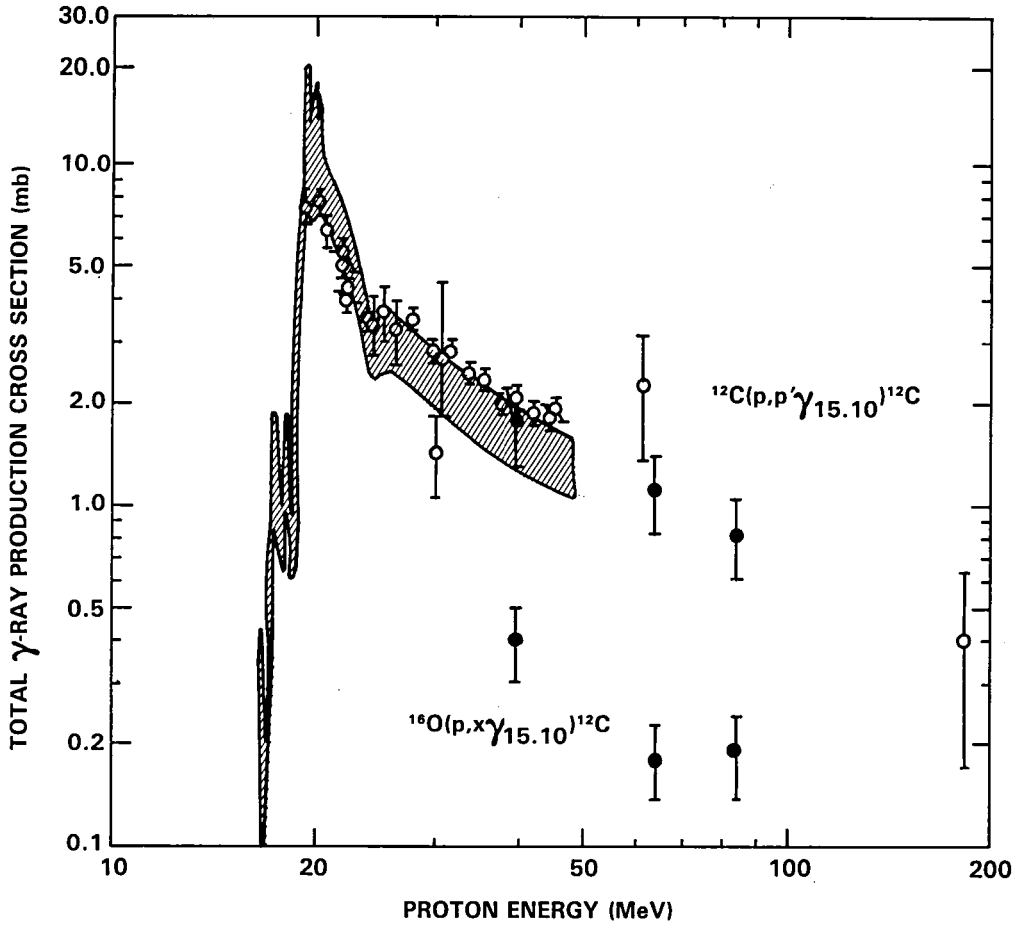

Figure 10. Production cross sections for 15.10-MeV gamma rays as a function of incident proton energy for the reactions $^{12}C(p,p'\gamma_{15.10})^{12}C$ (upper points and shaded region) and $^{16}O(p,x\ \gamma_{15.10})^{12}C$ (the lower three filled circles *only*). The upper three filled circles represent the present measurements for the CH_2 target. The shaded region represents the $\pm 20\%$ confidence interval of the differential gamma-ray production cross section measured at 90 degrees by Measday *et al.*[30] and Warburton and Funsten,[31] multiplied by 4π steradians for comparison with the total cross sections obtained in the present measurements. This neglects the fact that the gamma rays are not necessarily emitted isotropically. Angular fits to the present data for 40-, 65-, and 85-MeV incident protons indicate significant anisotropy in the gamma-ray emission. The apparent discrepancy between the excitation cross sections and the gamma-ray production cross sections could be explained by the degree of anisotropy observed. The open points represent measurements of the $^{12}C(p,p')^{12}C^*(15.11)$ excitation cross section, multiplied by the branching ratio for 15.10-MeV gamma rays of 0.9. References for the excitation cross sections are given in the text.

scattering from ^{12}C. For comparison, they normalized the gamma-ray production cross sections of Warburton and Funsten[31] and Measday *et al.*[30] to the excitation cross sections of Scott, Fisher, and Chant[32] for 21-MeV protons by multiplying by 0.8 and 0.9, respectively. As seen in Fig. 10, this normalization is not necessary to reconcile the gamma-ray production cross sections with the excitation cross sections. The observed systematic differences near 40 MeV are almost certainly due to anisotropic gamma-ray emission.

V.A.2. $^{16}O(p,x\ \gamma_{15.10})^{12}C$

The gamma-ray production cross sections for this reaction are presented in Table III and are plotted as the lower three filled circles in Fig. 10. Preliminary measurements of the ratio of this cross section to the cross section for the direct process $^{12}C(p,p'\gamma_{15.10})^{12}C$ by Lapides *et al.*[8] indicated that this ratio was comparable to the analogous ratio for producing 4.438-MeV gamma rays. From Table III, the ratio at 40 MeV for 15.10-MeV gamma rays is 0.227 ± 0.043, while for 4.438-MeV gamma rays the ratio is 0.697 ± 0.125, significantly larger. These ratios were taken to be equal by Crannell, Crannell, and Ramaty[4] in their computations for determining the spectral index of energetic protons responsible for 4.438- and 15.10-MeV line fluences from solar flares. The results presented here significantly alter the values of the spectral parameters determined in that work.

V.A.3. $^{16}O(p,p'\gamma_{6.129})^{16}O$

The present measurements of the gamma-ray production cross sections for this reaction are presented in Table III and are plotted in Fig. 11 as filled circles. These results have been normalized as described in Sec. IV.B. The crosses in Fig. 11 represent reported measurements of the gamma-ray production cross section by Dyer *et al.* for 8- to 23-MeV protons,[7] Narayanaswami *et al.* for 25- and 44-MeV protons,[38] Zobel *et al.* for 12.1-, 28.2-, 48.3-, and 145-MeV protons,[6] and Foley, Salmon, and Clegg for 146-MeV protons.[39] The results of Dyer *et al.* and Narayanaswami *et al.* were obtained with Germanium semiconductor detectors. Zobel *et al.* and Foley, Salmon, and Clegg reported values that are higher than these but, because they used NaI detectors with significantly poorer resolution, their results very likely include contributions due to unresolved gamma rays from the two single-nucleon knockout reactions $^{16}O(p,2p\ \gamma_{6.322})^{15}N$ and $^{16}O(p,x\ \gamma_{6.175})^{15}O$.

The open circles in Fig. 11 represent an estimate of the 6.129-MeV gamma-ray production cross section, obtained by summing the cross sections for the 6.130-, 8.872-, and 11.080-MeV levels multiplied by the appropriate branching ratios. Because the 3^+ state at 11.080 MeV cannot be resolved in (p,p') reactions from the 4^+ state at 11.095 MeV (which does not decay significantly through the 3^- level at 6.130 MeV), only the sum of the two excitation cross sections has been reported in the literature. Suzuki,[40] based on his calculations, has reported that the principal component of the wave function of both states consists of alpha-particle motion with $l = 2$ about the 2^+ excited state of ^{12}C. For this reason, it has been assumed in this work that the cross sections for excitation of these two states are equal.

Measurements of the 6.130-MeV excitation cross section have been reported by Daehnick for 17.0- and 18.8-MeV protons,[41] Hornyak and Sherr for 19-MeV protons,[42] Austin *et al.* for 23.4- to 46.1-MeV protons,[29] Amos *et al.*[21] and Kelley *et al.*[43] for 135-MeV protons, and Tyrén and Maris for 177-MeV protons.[44] Measurements of the 8.872-MeV cross sections have been reported by Daehnick for 17.0- and 18.8-MeV protons,[41] Hornyak and Sherr for 19-MeV protons,[42] Austin *et al.* for 23.4- to 46.1-MeV protons,[29] Perrin *et al.* for 42.5- and 44-MeV protons,[45] and Amos *et al.* for 135-MeV protons.[21] Measurements of the 11.080- plus 11.096-MeV excitation cross section have been reported by Hornyak and Sherr for 19-MeV protons[42] and Amos *et al.* for 135-MeV protons.[21] The 8.872-MeV level decays to the 6.130-MeV level 74% of the time.[46] The 11.08-MeV level decays directly to the 6.130-MeV level 34% of the time and decays indirectly to the 6.130-MeV level through the 8.872-MeV level less than 3% of the time.[47]

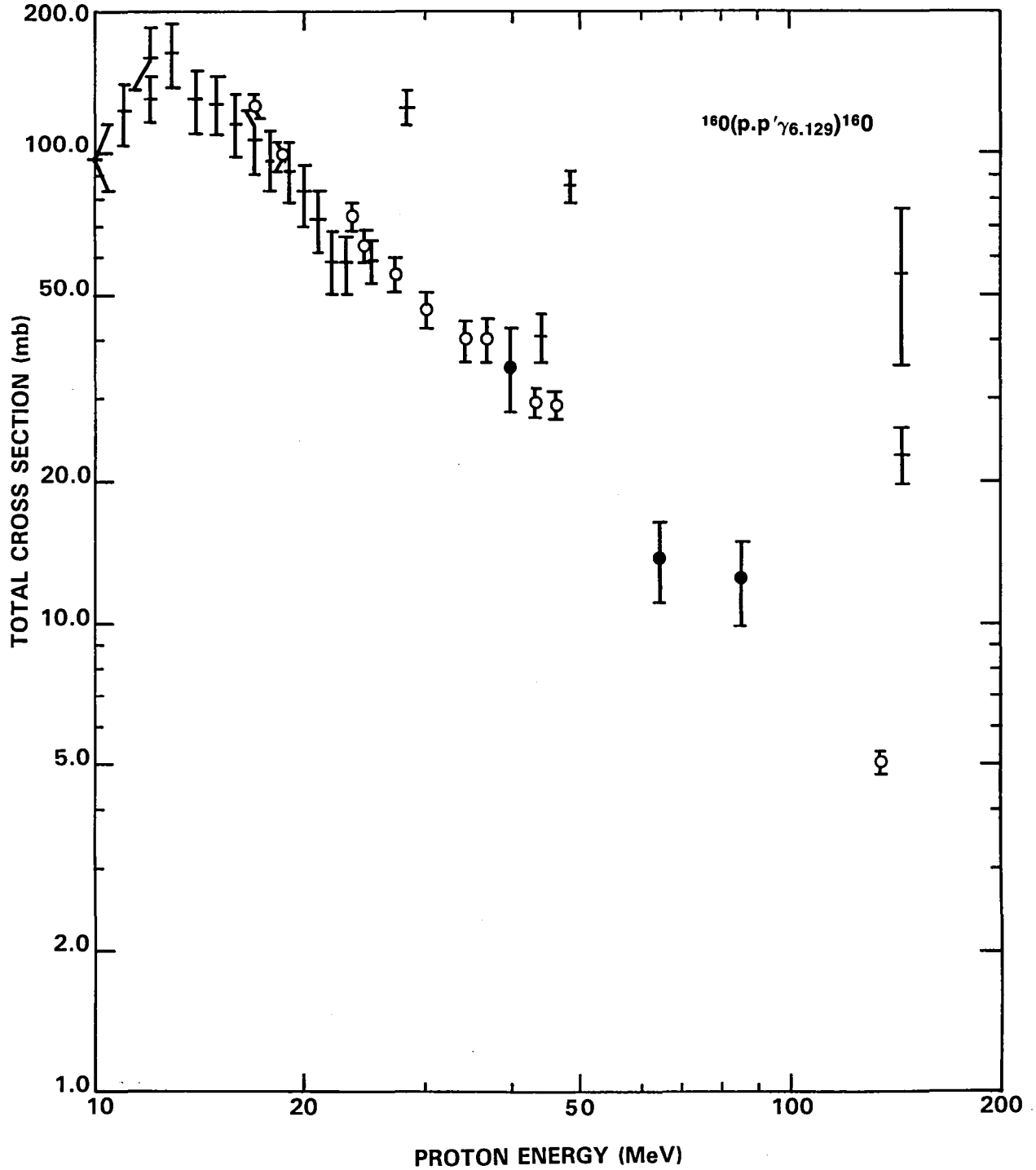

Figure 11. Production cross sections for 6.129-MeV gamma rays as a function of incident proton energy for the reaction $^{16}O(p,p'\gamma_{6.129})^{16}O$. The present measurements of the gamma-ray production cross sections are represented by filled circles. The crosses represent previously reported measurements of the gamma-ray production cross section. The open circles represent an estimate of the gamma-ray production cross sections derived from the 6.130-, 8.872-, and 11.080-MeV excitation cross sections. See text for further explanation and references.

V.A.4. $^{12}C(p,p'\ \gamma_{4.438})^{12}C$, $^{12}C(p,x\ \gamma_{2.000})^{11}C$, and $^{12}C(p,x\ \gamma_{2.154})^{10}B + {}^{12}C(p,2p\ \gamma_{2.124})^{11}B$

The first high-resolution measurements of the gamma-ray production cross sections for the reactions $^{12}C(p,x\ \gamma_{2.000})^{11}C$ and $^{12}C(p,x\ \gamma_{2.154})^{10}B + {}^{12}C(p,2p\ \gamma_{2.124})^{11}B$ were obtained in the present work and are presented in Table III. The latter two are not resolved, but the ^{10}B line is considerably weaker than the ^{11}B line. Zobel *et al.*[6] also measured a gamma-ray line near 2 MeV and attributed it entirely to the ^{11}C line. The results presented here indicate that they probably measured the summed cross section for the three lines from ^{11}C, ^{11}B, and ^{10}B, because these lines could not be resolved with their NaI detector. While the sum of the present measurements of these cross sections for 40-, 65-, and 85-MeV protons are systematically lower than the measurements of Zobel *et al.*, they are, individually, in agreement to within the experimental uncertainties.

Normalized cross section measurements for the production of 4.438-MeV gamma-rays from the bombardment of a ^{12}C target by protons are presented in Table III. They are also shown in Fig. 12 as filled circles. The crosses represent reported measurements of the gamma-ray production cross section by Dyer *et al.* for 6- to 23-MeV protons,[7] Zobel *et al.* for 14.6-, 30.3-, 50.3-, and 145-MeV protons,[6] and by Clegg *et al.* for 143-MeV protons.[48]

Because no higher-lying levels decay significantly through the 4.439-MeV level and because this level produces a 4.438-MeV gamma-ray 100% of the time, the excitation cross sections can be compared directly to the gamma-ray production cross sections. The 4.439-MeV excitation cross sections have been reported by Dickens, Haner, and Waddell for 31.1-MeV protons,[34] Stovall and Hintz for 39.8-MeV protons,[28] Fannon *et al.* for 49.5-MeV protons,[13] Strauch and Titus for 99.5-MeV protons,[49] Horowitz and Bell for 100-MeV protons,[50] Tyrén and Maris for 182-MeV protons,[44] and Hasselgren *et al.* for 185-MeV protons.[37] With the exception of Strauch and Titus, where there may have been problems resolving the 4.439-MeV peak from the elastic scattering peak, and Zobel *et al.*, all results are remarkly consistent with a power-law decrease of the cross section with energy for proton energies greater than about 15 MeV. Ramaty, Kozlovsky, and Lingenfelter[12] suggested that the difference between the gamma-ray production cross sections of Zobel *et al.* and the collected excitation cross sections was due to the unresolved contributions of gamma rays from the $^{12}C(p,2p\ \gamma_{4.444})^{11}B$ reaction. Because both this line and the 4.438-MeV line are broadened due to Doppler shifts, this was a plausable explanation. That this is no longer the case, based on additional information and further considerations, is developed in the remainder of this subsection.

Similarities at $E_p = 100$ MeV in the angular distribution[54] of symmetric protons from the reactions $^{12}C(p,2p)^{11}B^*(E_n)$, n = 1–5 (as well as from the ground state) suggest that the dominant reaction mechanism is proton knock-out. While the ^{11}B excited states were not the object of a similar analysis in an earlier (p,2p) experiment[55] for 50-MeV protons, the angular distributions are qualitatively similar so that down to incident proton energies of about 40 MeV, a proton knock-out or quasi-free p-p scattering mechanism can be assumed. In that case, the cross section for producing a given $^{11}B^*$ excited state is proportional to $[C_s(E_n)]^2\sigma_{pp}$, where $[C_s(E_n)]^2$ is the relative spectroscopic factor for a $^{11}B^*(E_n)$ + p component being present in the ^{12}C ground state wave function. The total cross section for producing the analogue $^{11}C^*(E_n)$ state is proportional to $[C_s(E_n)]^2\sigma_{pn}$, where the spectroscopic factor is the same but the proton-neutron cross section replaces the proton-proton. The ratio of a given (p,2p) reaction to its analogue (p,pn) should be given by the ratio σ_{pp}/σ_{pn}, which is approximately one third at the energies of interest to the present experiment.

It must be stressed that the ratios of gamma-ray production cross sections from analogue states can depart widely from the ratio σ_{pp}/σ_{pn} because the gamma-ray cascades "feeding" the pair of states in question may differ radically. For example, for 1-GeV incident protons, Goryachev *et al.*[25] report a ratio of about two for

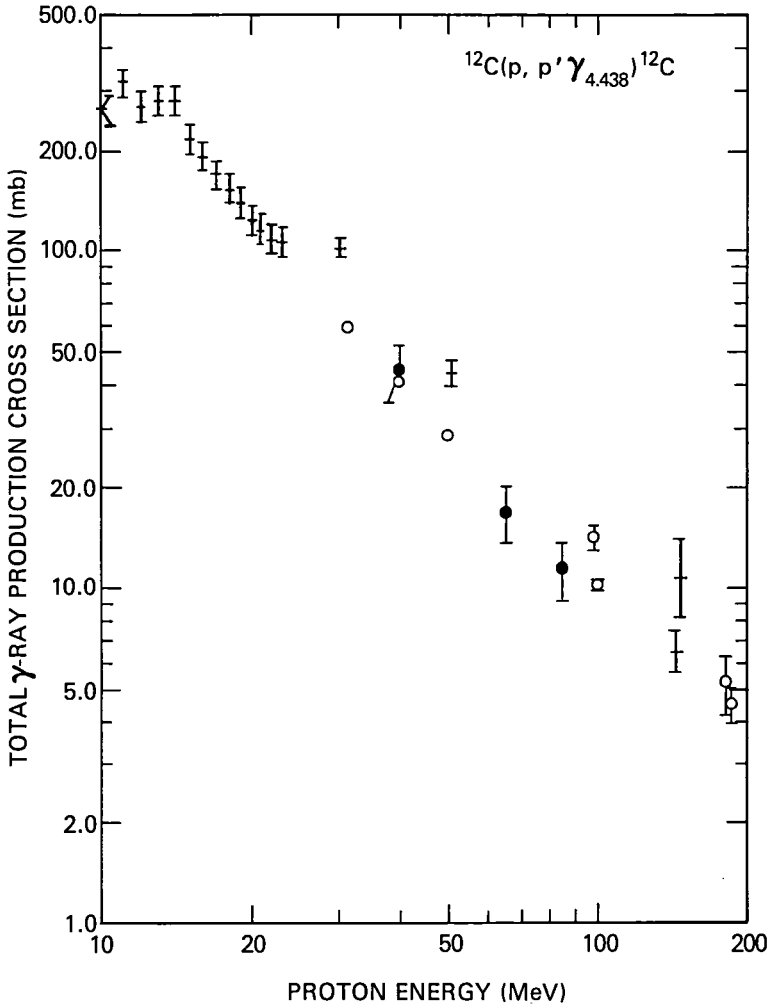

Figure 12. Production cross section for 4.438-MeV gamma rays as a function of incident proton energy for the reaction $^{12}C(p,p'\gamma_{4.438})^{12}C$. The present measurements are represented by filled circles. The crosses represent previously reported measurements of the gamma-ray production cross section. The open circles represent measurements of the scattered protons in the (p,p') reaction, integrated to give total excitation cross sections which, for the 4.439-MeV state of ^{12}C, are equal to the 4.438-MeV gamma-ray production cross section. References are given in the text.

$\sigma[^{16}O(p,2p\ \gamma_{6.322})^{15}N]/\sigma[^{16}O(p,x\ \gamma_{6.175})^{15}O]$, while the ratio σ_{pp}/σ_{pn} is 1.2. The reason is that there are significant cascades to the $^{15}N(3/2^-, 6.324)$ state which originate from analogue states that are unbound against particle decay in ^{15}O but that are bound in ^{15}N. In the A = 11 system, however, there are effectively the same number of bound states in ^{11}B as in ^{11}C and the gamma-ray branching ratios are very similar.[24] Advantage is taken of this situation to estimate the gamma-ray production cross section for the $^{12}C(p,2p\ \gamma_{4.444})^{11}B$ reaction from the reported cross sections for the $^{12}C(p,2p\ \gamma_{2.124})^{11}B$ and $^{12}C(p,x\ \gamma_{2.000})^{11}C$ reactions.

The relative spectroscopic factors for knock-out of a p-state proton leaving the residual ^{11}B in the $1/2^-$ (2.125), $5/2^-$ (4.445), $3/2^-$ (5.020), and $7/2^-$ (6.743) states have been reported for 100-MeV incident protons.[54] In addition, the ratio of the cross section for exciting the $1/2^+$ (6.792) state to that of the $1/2^-$ (2.125) state was estimated from the triply differential cross sections reported by Pugh *et al.*,[55] where most of the strength going to the unresolved line centered at 6.76 MeV is due to the $1/2^+$. In Table IV, the relative cross sections for

Table IV. Relative cross sections for exciting the lowest five states in ^{11}B through the $^{12}C(p,2p)^{11}B^*$ reaction.

State	Energy (MeV)	$\sigma(E_n)/\sigma(2.125)$
$1/2^-$	2.125[a]	1
$3/2^-$	4.445[a]	0.3
$5/2^-$	5.020[a]	1
$1/2^+$	6.792[b]	2.3
$7/2^-$	6.743[a]	0.18

[a] Table 3 of Ref. 54.

[b] Figure 8 of Ref. 55.

exciting these states are tabulated. This table, together with gamma-ray branching ratios reported in the literature, allow the desired ratio $\sigma[^{12}C(p,2p\ \gamma_{4.444})^{11}B]/\sigma[^{12}C(p,2p\ \gamma_{2.124})^{11}B]$ to be estimated to be about 0.2.

Because the narrow $^{10}B^*(2.154)$ gamma-ray line makes a small but unresolved contribution to the broad $^{11}B^*(2.125)$ line in the present experiment, the line from $^{11}C^*(2.000)$ is also used by normalizing it to the equivalent line from $^{11}B^*(2.124)$ through multiplication by σ_{pp}/σ_{pn}. This ratio varies smoothly from 0.33 for 40-MeV incident protons to 0.35 for 85-MeV incident protons. In Table V are shown the two estimates of the $^{12}C(p,2p\ \gamma_{4.444})^{11}B$ cross section at the three proton energies of interest. A similarly small cross section has also been estimated from a qualitative examination of the $^{11}C(5/2^-, 4.803)$ and $^{11}B(5/2^-, 5.019)$ gamma-ray lines observed in this experiment.

The largest value of the $^{11}B(\gamma_{4.444})$ cross section, estimated for 40-MeV protons, is 1.22 ± 0.25 mb. If the 4.4-MeV gamma-ray production cross section of Zobel *et al.*[6] is assumed to decrease as a power-law with energy from 30 to 50 MeV and if it is assumed that the gamma rays are emitted isotropically [this gives a lower limit to the total cross section since the differential cross section for the $^{12}C(p,p'\gamma_{4.438})^{12}C$ reaction is seen to be a minimum at 90 degrees in Fig. 9], then the total gamma-ray production cross section for 40-MeV protons is estimated to be 64.4 ± 3.5 mb. This is 22 ± 4 mb higher than the excitation cross section of 42.9 ± 1.0 mb estimated from the measurements of Stovall and Hintz.[28] Because this value is significantly higher than

Table V. Estimates of the gamma-ray production cross section for $^{12}C(p,2p\ \gamma_{4.444})^{11}B$ obtained by multiplying two different values for the $^{12}C(p,2p\ \gamma_{2.125})^{11}B$ cross section by 0.2. The two values were obtained as follows: (1) The present $^{12}C(p,2p\ \gamma_{2.000})^{11}C$ cross section was multiplied by σ_{pp}/σ_{pn}, and (2) The ^{11}B cross section was measured directly, but a small contribution from $^{12}C(p,x\ \gamma_{2.154})^{10}B$ was not removed.

E_p (MeV)	$\sigma_{TOT}(\gamma_{2.000})$ experimental (mb)	$\sigma_{TOT}(\gamma_{2.124})$ theoretical (1) (mb)	$\sigma_{TOT}(\gamma_{4.444})$ theoretical (1) (mb)	$\sigma_{TOT}(\gamma_{2.124})$ experimental (2) (mb)	$\sigma_{TOT}(\gamma_{4.444})$ experimental (2) (mb)
40	12.4 ± 2.5	4.09 ± 0.83	0.82 ± 0.16	6.11 ± 1.27	1.22 ± 0.25
65	9.8 ± 2.0	3.33 ± 0.68	0.67 ± 0.14	4.86 ± 1.03	0.97 ± 0.21
85	9.1 ± 1.9	3.19 ± 0.66	0.64 ± 0.13	4.83 ± 1.02	0.97 ± 0.20

the 1.22 ± 0.25 mb estimated for the $^{12}C(p,2p\ \gamma_{4.444})^{11}B$ reaction, this reaction cannot account for the discrepancy between the gamma-ray production cross sections of Zobel *et al.* and the collected excitation cross sections.

V.A.5. $^{16}O(p,x\ \gamma_{4.438})^{12}C$

The 4.438-MeV gamma-ray production cross section for this reaction was obtained only for 40-MeV protons (see Sec. IV.A.3) and is presented in Table III. The normalized value is also plotted in Fig. 13. Also shown in Fig. 13 are the reported gamma-ray production cross sections of Dyer *et al.* for 14- to 23-MeV protons,[7] Zobel *et al.* for 12.1-, 28.2-, 48.3-, and 145-MeV protons,[6] and Foley, Salmon, and Clegg for 146-MeV protons.[39] No particle measurements were found in the literature for this 3-body final state reaction.

Reported measurements of the 4.438-MeV gamma-ray production cross section for p + ^{16}O above E_p = 23 MeV by Zobel *et al.*[6] are differential cross sections at 135 degrees. They report values of 8.7 ± 0.7 mb/sr

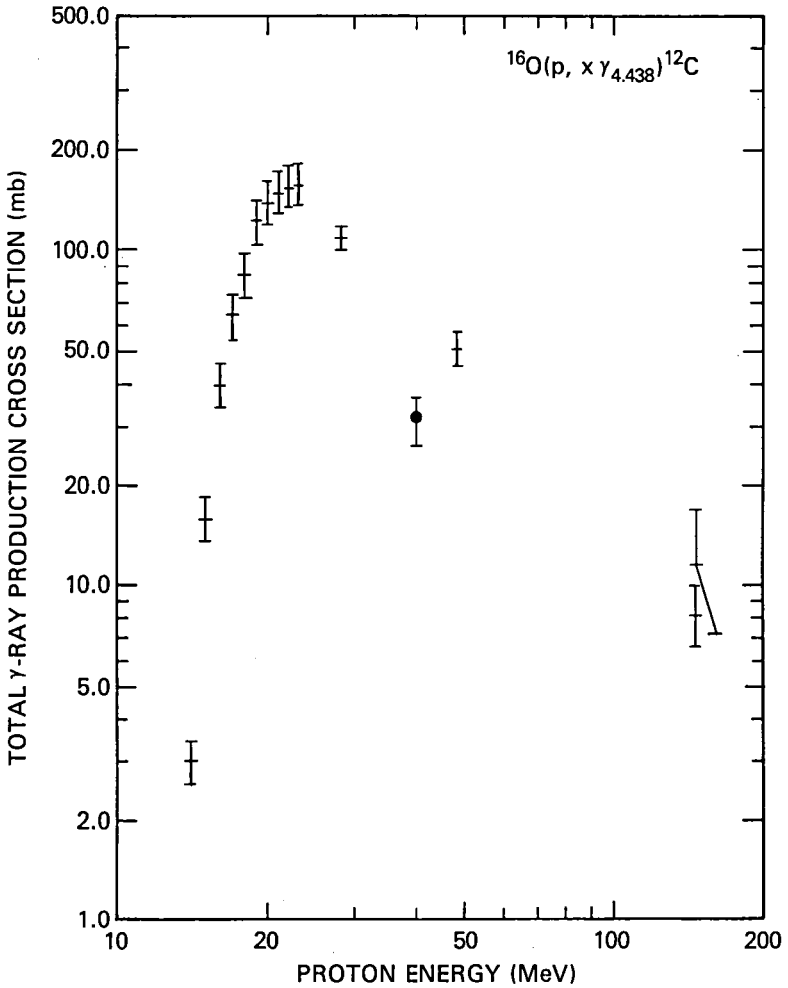

Figure 13. Production cross section for 4.438-MeV gamma rays as a function of incident proton energy for the reaction $^{16}O(p,x\ \gamma_{4.438})^{12}C$. The present measurement is represented by a filled circle. The crosses represent other reported measurements of the gamma-ray production cross section. References are given in the text.

for 28.2-MeV protons and 4.0 ± 0.4 mb/sr for 48.3-MeV protons. If the cross section is assumed to decrease as a power-law with energy between these proton energies and if it is assumed that the gamma rays are emitted isotropically (not an unreasonable assumption based on the angular distribution presented in Fig. 9), then the total gamma-ray production cross section for 40-MeV protons is estimated to be 66.0 ± 4.7 mb. This is significantly higher than the value of 31.1 ± 5.9 mb derived in the present work.

An independent estimate of the gamma-ray production cross section for 45-MeV protons can be obtained directly from the α_1 widths and the (p,p') cross sections as follows:

$$\sigma = \left[\sum_N \frac{\Gamma_{\alpha 1}(E_N)}{\Gamma_{tot}(E_N)}\,\sigma(40°,E_N)\right] \int d\Omega_c \frac{\sigma(\theta_c,21\text{–}27\ \text{MeV})}{\sigma(40°,21\text{–}27\ \text{MeV})}\,, \tag{37}$$

where the integral is performed over all solid angles and the sum is over all ^{16}O excited states that contribute to the reaction. The estimate of the cross section made this way is $26.6^{+8.7}_{-4.6}$ mb and is in good agreement with the normalized value for 40-MeV incident protons of 31.1 ± 5.9 mb. The angular distribution of Buenerd *et al.*[16] for $21 \leq E_N \leq 27$ MeV was used to carry out the integral and the confidence interval was estimated by calculating the contribution to the cross section for states above 16 MeV with $\Gamma_{\alpha 1}/\Gamma_{tot} = 0.5$ and 0.25.

V.A.6. $^{16}O(p,2p\ \gamma_{5.269})^{15}N$, $^{16}O(p,x\ \gamma_{5.240})^{15}O$, and $^{16}O(p,x\ \gamma_{5.105})^{14}N$

The normalized gamma-ray production cross sections for these three reactions are presented in Table III. These three narrow lines are readily discernible in the raw pulse-height spectra (see Fig. 6). Despite the use of a high-resolution gamma-ray detector, the two Doppler broadened lines from ^{15}N and ^{15}O at 5.298 and 5.182 MeV, respectively, were not resolved.

Zobel *et al.*[6] reported measurements of the differential cross section for a gamma-ray line near 5.1 to 5.2 MeV of 5.8 ± 0.5, 4.1 ± 0.5, and 0.96 ± 0.39 mb/sr for protons of energy 28.2, 48.3, and 145 MeV, respectively, incident on an oxygen target. In that work it was suggested that this line arose from the (p,p'n) and (p,2p) reactions with ^{16}O. It is likely that the four lines (two from each of ^{15}N and ^{15}O) near 5.25 MeV, as well as the 5.105-MeV line from the $^{16}O(p,x\ \gamma_{5.105})^{14}N$ reaction, contributed to the single line observed by Zobel *et al.*

If isotropic gamma-ray emission is assumed, the total gamma-ray production cross section can be estimated from the results of Zobel *et al.*[6] Under the assumption that the cross section decreases as a power law with energy between each measurement of Zobel *et al.*, the cross section is estimated to be 58.2 ± 4.9, 34.8 ± 4.9, and 24.4 ± 5.3 mb, for 40-, 65-, and 85-MeV protons, respectively. For comparison, if the three resolved normalized cross sections reported in Table III are summed, the totals are 33.4 ± 4.1, 19.4 ± 2.3, and 14.3 ± 1.8 mb for 40-, 65-, and 85-MeV protons, respectively. Some, if not all, of the difference between these cross sections and the values extrapolated from the reported cross sections of Zobel *et al.* is due to the two unresolved lines.

Foley, Salmon, and Clegg[39] have observed a gamma-ray line at 5.25 MeV produced by 146-MeV protons incident on ^{16}O. The gamma-ray production cross section reported for this line was 2.6 ± 0.7 mb. Foley, Salmon, and Clegg suggested that it arose from the four lines of ^{15}O and ^{15}N near 5.25 MeV. If the logarithm of the normalized cross sections obtained in this work, presented in Table III, for the sum of the three resolved lines for 65- and 85-MeV protons is assumed to decrease as a power law with proton energy and is extrapolated to 146 MeV, a cross section of 7.7 ± 3.5 mb is obtained. This value is higher than the results of Foley, Salmon, and Clegg for the total of all five lines, but has a large uncertainty.

The only other measurement of the gamma-ray production cross section for any of these five lines is an upper limit of 15 mb for 23-MeV protons for the 5.269-MeV line reported by Dyer *et al.*[7] As this is only 4.5

MeV above threshold (the maximum cross section should occur for 25- to 26-MeV protons), the results reported here cannot be extrapolated for direct comparison.

V.A.7. $^{16}O(p,x\ \gamma_{2.793})^{14}N^*(2.313)$, $^{16}O(p,x\ \gamma_{2.313})^{14}N$, and $^{16}O(p,p'\gamma_{2.740})^{16}O^*(6.130)$

The 2.793-MeV gamma rays observed in this work arise from the decay of the 5.106-MeV level of ^{14}N to the 2.313-MeV level. The branching ratio for this decay is 0.194 ± 0.012, while the ratio for decay to the ground state is 0.799 ± 0.010.[51] If the 2.793-MeV and 5.105-MeV gamma-ray production cross sections are divided by the corresponding branching ratios, the resulting cross sections are statistically self-consistent for each proton energy.

The 2.741-MeV gamma rays arise from the decay of the 8.872-MeV level of ^{16}O to the 6.130-MeV level, with a branching ratio of 0.760 ± 0.030 to the 6.130-MeV level and a branching ratio of only 0.072 ± 0.008 to the ground state.[18] If the normalized 2.741-MeV gamma-ray production cross section is divided by the branching ratio for producing these gamma rays, the total cross section for producing the 8.872-MeV state is obtained. This value includes the direct contribution as well as the contribution due to cascades from higher-lying levels. When this is done, values for the excitation cross sections of 3.61 ± 0.42, 2.30 ± 0.28, and 1.80 ± 0.23 mb for 40-, 65-, and 85-MeV protons, respectively, are obtained.

Austin *et al.* have reported total excitation cross sections for the reactions $^{16}O(p,p')^{16}O^*(6.130$ and $8.872)$ by protons with energies from 23 to 46 MeV.[29] At 40 MeV, a cross section of 32 ± 2 mb for the direct excitation of the 6.130-MeV level and 3.2 ± 0.3 mb for the direct excitation of the 8.872-MeV level are obtained from Fig. 4 of Austin *et al.* This latter number, multiplied by the branching ratio to the 6.130-MeV level, gives the contribution of the direct excitation of the 8.872-MeV level to the 2.741-MeV gamma-ray production cross section of 2.4 ± 0.2 mb. This is statistically consistent with the normalized 2.741-MeV gamma-ray production cross section from Table III of 2.74 ± 0.30.

The 2.313-MeV gamma rays from ^{14}N can be produced from the $^{16}O(p,x\ \gamma_{2.313})^{14}N$ reaction as well as through cascades from higher levels of ^{14}N excited by a similar reaction. The 3.948-MeV level decays 96.1% of the time to the 2.313-MeV level, producing a 1.635-MeV gamma ray. A peak at 1.635 MeV is clearly observed in the measured pulse-height spectra. The cross sections for this peak cannot be determined, however, because at least three nearby lines mutually overlap it. Note that the 5.106-MeV state provides a contribution to the 2.313-MeV cross section which is equal to the cross section for production of 2.793-MeV gamma rays. As is seen in Table III, this contribution is less than 10% of the total cross section for 2.313-MeV gamma rays.

Zobel *et al.* reported gamma-ray production cross sections for a line with an energy of about 2.2 to 2.35 MeV.[6] They suggested that these gamma rays were produced by the $^{16}O(p,x\ \gamma_{2.365})^{13}N$ reaction. If the cross section is assumed to decrease as a power law with proton energy between the measurements of Zobel *et al.*[6] for 28.2-, 48.3-, and 145-MeV protons, the gamma-ray production cross sections for 40-, 65-, and 85-MeV protons can be estimated to be 9.5 ± 3.1, 6.4 ± 1.8, and 5.1 ± 1.5 mb, respectively. These values are in good agreement with the normalized 2.313-MeV gamma-ray production cross sections from ^{14}N presented in Table III. For this reason, Ramaty, Kozlovsky, and Lingenfelter[12] are probably correct when they suggested that Zobel *et al.* did not measure gamma rays from the decay of ^{13}N as reported but from the decay of ^{14}N.

V.B. Summary and conclusions

In this work, the gamma-ray production cross sections for a large number of lines resulting from interactions of protons with ^{12}C and ^{16}O targets have been measured for incident proton energies of 40, 65, and

85 MeV. These cross sections are presented in Table III. An accurate knowledge of these cross sections from threshold to proton energies of 100 MeV or greater is important for the interpretation of a wide variety of space physics observations. The measured gamma-ray production cross sections from the present experiment for the most important lines, either by virtue of their large gamma-ray energy, such as the $^{12}C^*(15.11)$, or by virtue of their large production cross sections, such as the $^{16}O^*(6.130)$ and the $^{12}C^*(4.439)$, are compared with earlier measurements in Figs. 10, 11, 12, and 13.

With regard to the $^{12}C(p,p'\gamma_{15.10})^{12}C$ cross section, the data presented in Fig. 10 demonstrate that after the present differential cross section at 90° is normalized to the 90° measurement of Measday *et al.*,[30] and the slightly anisotropic angular distribution measured in the current experiment is adopted, the new 40-MeV point is in excellent agreement with the production cross section derived from the proton excitation cross section measured by Geramb *et al.*[33] Crannell, Crannell, and Ramaty[4] presented smoothed curves representing the 15.11-MeV excitation cross sections reported in the literature. They also estimated excitation cross sections from gamma-ray production cross sections by normalizing the latter to the excitation measurement of Scott, Fisher, and Chant[32] for 21-MeV protons. This, however, led to an apparent factor of two difference between the two curves for 50-MeV incident protons.[4] Because the present work indicates that the results of gamma-ray production experiments and the results of excitation experiments are in reasonable agreement for 50-MeV incident protons, the normalization performed by Crannell, Crannell, and Ramaty of all measurements at 21 MeV has not been imposed on the data in Fig. 10. The $^{16}O(p,x\ \gamma_{15.10})^{12}C$ cross section points plotted in the same figure are the first such measurements reported in the literature. At the given energies this cross section is approximately 20% that of the $^{12}C(p,p'\gamma_{15.10})^{12}C$.

The present $^{16}O(p,x\ \gamma_{6.129})^{16}O$ cross sections, plotted in Fig. 11, follow closely the trend of previous gamma-ray production measurements as well as gamma-ray production cross sections deduced from excitation experiments. In extracting the latter, one must take into account the contribution from the decay of the $^{16}O^*(2^+,8.872)$ and $^{16}O^*(3^+,11.080)$ levels to the $^{16}O^*(3^-,6.130)$ level. The points from the work of Zobel *et al.*,[6] which tend to be about a factor of three higher, should not be compared directly. Those measurements were taken with a NaI detector which could not resolve the $^{16}O^*(6.130)$ line from the strongly excited $^{15}N^*(6.324)$ and $^{15}O^*(6.176)$ lines.

The present measurements of the $^{12}C(p,p'\gamma_{4.438})^{12}C$ cross section are presented in Fig. 12. The gamma-ray production cross section for 40-MeV protons was normalized to the 43 ± 1 mb excitation cross section of Stovall and Hintz[28] at the same energy. This was done on the basis of the argument presented in Sec. V.A.4 that there are no significant contributions from unresolved lines, particularly the 4.444-MeV line from $^{11}B^*(4.445)$ as proposed by Ramaty, Kozlovsky, and Lingenfelter.[12] The gamma-ray production cross sections of Zobel *et al.*[6] are about a factor of 1.5 higher than the excitation cross sections. This difference amounts to 22 ± 4 mb for 40-MeV protons and far exceeds the 1.2 mb estimated in Sec. V.A.4 for the $^{12}C(p,2p\ \gamma_{4.444})^{11}B$ reaction.

A comparison is made in Fig. 13 of the $^{16}O(p,x\ \gamma_{4.438})^{12}C$ cross section for 40-MeV protons with previously reported results. Again the measurement of Zobel *et al.*[6] for 50-MeV protons is higher, by about a factor of two, than the present measurement at 40 MeV, but, until additional results are reported it is impossible to select one measurement over the other. Because the spallation production of gamma rays proceeds through a particle three-body final state, no excitation cross section measurements are available. The effort required in making a complete kinematic determination (one that includes all phase space) is prohibitive. The raw data collected for the present experiment for 65- and 85-MeV protons await the calculation of a "template," which requires differential cross sections for inelastic proton scattering to $^{16}O^*$ at similar incident proton energies not currently available in the literature.

Murphy[52] has studied relative isotopic abundances at the site of solar flares using spectra measured with the Gamma-Ray Spectrometer (GRS) on board the Solar Maximum Mission (SMM) satellite. He concludes first that the most likely site of the interaction is in the solar chromosphere and second that the abundances of ^{12}C and ^{16}O are lower than those in the solar photosphere by factors of three or four. The latter result is insensitive to the assumed particle spectrum.[52] This suppression has also been observed by Meyer, who suggests that it may be caused by charge-dependent mass transport from the photosphere to the corona based on first-ionization potential.[53] For a reasonable proton spectrum,[52] the use of the present gamma-ray production cross sections can lead to no more than a 25% increase in the ^{12}C and ^{16}O abundances when compared with abundances derived[52] using the cross sections of Zobel *et al.*[6] While this increase is not sufficient to account for the reported abundance deficits, further measurements of the $^{16}O(p,x\ \gamma_{4.438})^{12}C$ gamma-ray production cross section from threshold, 12.3 MeV, through 100 MeV are required to determine the solar abundances to the desired accuracy.

Future observations of high-energy gamma rays from solar flares will provide an opportunity to investigate the spectrum of accelerated particles, which in turn can be used to gain information about the acceleration mechanism. A thorough knowledge of relevant cross sections is critical for the interpretation of such spectra. The gamma-ray production cross sections for the reactions $^{12}C(p,p'\gamma_{4.438})^{12}C$ and $^{12}C(p,p'\gamma_{15.10})^{12}C$ are now reasonably well-determined for proton energies up to 200 and 100 MeV, respectively. This is not the case for the production of the same lines from ^{16}O. The results obtained in the present work indicate that the flux ratio of 4.438-MeV to 15.10-MeV gamma rays is significantly different for the two nuclei so that the flux ratio produced in solar flares is both abundance and proton-spectrum dependent. Further measurements of the 15.10-MeV gamma-ray production cross section for p + ^{16}O are necessary both for confirmation of the present results and for extension of these to higher proton energies and to lower energies, especially between the threshold at 23.7 MeV and 40 MeV.

VI. ACKNOWLEDGEMENTS

The possibility of obtaining the measurements reported here using the University of Maryland Cyclotron was first recognized and brought to the attention of two of the authors (CJC and JIT) by Dr. N. S. Wall, Professor of Physics at the University of Maryland, who participated in and encouraged this work until his unexpected death on September 2, 1979. His key role at the inception of these efforts is gladly acknowledged, and his continued participation as a friend and collaborator is sadly missed. The efforts of the cyclotron administration and staff in providing accelerator time and data-acquisition facilities are gratefully acknowledged. The germanium detector employed in these measurements was provided by Princeton Gamma Tech (PGT) under time constraints which were extraordinarily severe. The cooperation and responsiveness of the PGT staff are, likewise, sincerely appreciated. Additional assistance was provided by a number of individuals whose contributions are acknowledged as follows. Dr. N. R. Yoder was indispensible in providing help with software programming for data acquisition at the cyclotron. Mr. S. M. Seltzer calculated the response of the detector employed in this work to gamma rays with energies throughout the range of interest. Dr. L. G. Evans, assisted by Ms. J. V. Stoakes, applied HYPERMET for reduction of the raw spectral data. Further assistance with data acquisition and reduction was supplied by Dr. M. J. Bielefeld, Dr. J. R. Lapides, Dr. C. Samantha, Mr. R. L. Schmadebeck, Dr. L. W. Wo, Dr. L. I. Yin, Mr. D. Okamoto, Mr. C. Wade, and several enthusiastic summer students. Dr. H. Crannell and Dr. J. R. Calarco participated in valuable discussions on experimental technique and the physics of the nuclear transitions being studied. Dr. H. Crannell

also provided valuable comments on earlier versions of this manuscript. Two of us (FLL and CWW) gratefully acknowledge support for this work provided in part through NASA grant NSG 5066.

VII. REFERENCES

(1) E. L. Chupp, in *Annual Review of Astronomy and Astrophysics*, edited by G. Burbidge, D. Layzer, and J. G. Phillips (Annual Reviews Inc., Palo Alto, 1984), p. 359.
(2) E. L. Chupp, D. J. Forrest, P. R. Higbie, A. N. Suri, C. Tsai, and P. P. Dunphy, Nature (London) *241*, 333 (1973).
(3) R. E. Lingenfelter and R. Ramaty, in *High-Energy Nuclear Reactions in Astrophysics*, edited by B. S. P. Shen (Benjamin, New York, 1967), p. 99.
(4) C. J. Crannell, H. Crannell, and R. Ramaty, Astrophys. J. *229*, 762 (1979).
(5) R. W. Noyes, *The Sun* (Harvard University, Cambridge, 1982), p. 44.
(6) W. Zobel, F. C. Maienschein, J. H. Todd, and G. T. Chapman, Nucl. Sci. Eng. *32*, 392 (1968).
(7) P. Dyer, D. Bodansky, A. G. Seamster, E. B. Norman, and D. R. Maxson, Phys. Rev. C *23*, 1865 (1981).
(8) J. R. Lapides, C. J. Crannell, H. Crannell, W. F. Hornyak, S. M. Seltzer, J. I. Trombka, and N. S. Wall, NASA Technical Memorandum No. 79560, 1978.
(9) S. M. Seltzer (private communication).
(10) J. J. Kolata, R. Auble, and A. Galonsky, Phys. Rev. *162*, 957 (1967).
(11) J. D. Jackson, *Classical Electrodynamics*, 2nd. ed. (Wiley, New York, 1975), p. 753.
(12) R. Ramaty, B. Kozlovsky, and R. E. Lingenfelter, Astrophys. J. Suppl. Ser. *40*, 487 (1979).
(13) J. A. Fannon, E. J. Burge, D. A. Smith, and N. K. Ganguly, Nucl. Phys. A *97*, 263 (1967).
(14) T. A. Carey, P. G. Roos, N. S. Chant, A. Nadasen, and H. L. Chen, Phys. Rev. C *29*, 1273 (1984).
(15) M. B. Epstein, J. R. Quinn, S. N. Bunker, J. W. Verba, and J. R. Richardson, Nucl. Phys. A *169*, 337 (1971).
(16) M. Buenerd, P. Martin, P. de Saintignon, and J. M. Loiseaux, Phys. Rev. C *14*, 1316 (1976).
(17) Charles Earl Hyde-Wright, Ph.D. thesis, Massachusetts Institute of Technology, 1984.
(18) F. Ajzenberg-Selove, Nucl. Phys. A *375*, 1 (1982).
(19) K. H. Bray, A. D. Frawley, T. R. Ophel, and F. C. Barker, Nucl. Phys. A *288*, 334 (1977).
(20) P. Martin and T. R. Ophel, Nucl. Phys. A *202*, 257 (1973).
(21) K. Amos, W. Bauhoff, I. Morrison, S. F. Collins, R. S. Henderson, B. M. Spicer, G. G. Shute, V. C. Officer, D. W. Devins, D. L. Friesel, and W. P. Jones, Nucl. Phys. A *413*, 255 (1984).
(22) A. D. Frawley, K. H. Bray, and T. R. Ophel, Nucl. Phys. A *294*, 161 (1978).
(23) H. R. Weller, H. A. van Rinsvelt, and F. E. Dunnam, Phys. Lett. *27B*, 283 (1968).
(24) C. P. Browne, W. A. Schier, and I. F. Wright, Nucl. Phys. *66*, 49 (1965).
(25) W. J. O'Connell, Ph.D. thesis, Stanford, 1969; data reproduced in H. D. Shay, R. E. Peschel, J. M. Long, and D. A. Bromley, Phys. Rev. C *9*, 76 (1974).
(26) G. W. Phillips and K. W. Marlow, Nucl. Instrum. Methods *137*, 525 (1976).
(27) J. I. Trombka and R. L. Schmadebeck, Nucl. Instrum. Methods *62*, 253 (1968).
(28) T. Stovall and N. M. Hintz, Phys. Rev. *135*, B330 (1964).
(29) S. M. Austin, P. J. Locard, S. N. Bunker, J. M. Cameron, J. R. Richardson, J. W. Verba, and W. T. H. van Oers, Phys. Rev. C *3*, 1514 (1971).
(30) D. F. Measday, P. S. Fisher, A. Kalmykov, F. A. Nikolaev, and A. B. Clegg, Nucl. Phys. *45*, 98 (1963).

(31) E. K. Warburton and H. O. Funsten, Phys. Rev. *128*, 1810 (1962).
(32) D. K. Scott, P. S. Fisher, and N. S. Chant, Nucl. Phys. A *99*, 177 (1967).
(33) H. V. Geramb, K. Amos, R. Sprickmann, K. T. Knöpfle, M. Rogge, D. Ingham, and C. Mayer-Böricke, Phys. Rev. C *12*, 1697 (1975).
(34) J. K. Dickens, D. A. Haner, and C. N. Waddell, Phys. Rev. *129*, 743 (1963).
(35) E. L. Petersen, I. Slaus, J. W. Verba, R. F. Carlson, and J. R. Richardson, Nucl. Phys. A *102*, 145 (1967).
(36) K. A. Amos, H. V. Geramb, R. Sprickmann, J. Arvieux, M. Buenerd, and G. Perrin, Phys. Lett. *52B*, 138 (1974).
(37) D. Hasselgren, P. U. Renberg, O. Sundberg, and G. Tibell, Nucl. Phys. *69*, 81 (1965).
(38) J. Narayanaswamy, P. Dyer, S. R. Faber, and S. M. Austin, Phys. Rev. C *24*, 2727 (1981).
(39) K. J. Foley, G. L. Salmon, and A. B. Clegg, Nucl. Phys. *31*, 43 (1962).
(40) Y. Suzuki, Prog. Theor. Phys. *55*, 1751 (1976).
(41) W. W. Daehnick, Phys. Rev. *135*, B1168 (1964).
(42) W. F. Hornyak and R. Sherr, Phys. Rev. *100* 1409 (1955).
(43) J. Kelly, W. Bertozzi, T. N. Buti, F. W. Hersman, C. Hyde, M. V. Hynes, B. Norum, F. N. Rad, A. D. Bacher, G. T. Emery, C. C. Foster, W. P. Jones, D. W. Miller, B. L. Berman, W. G. Love, and F. Petrovich, Phys. Rev. Lett. *45*, 2012 (1980).
(44) H. Tyrén and T. A. J. Maris, Nucl. Phys. *4*, 637 (1957).
(45) G. Perrin, D. Lebrun, J. Chauvin, P. Martin, P. De Santignon, D. Eppel, H. V. Geramb, H. L. Yadav, and V. A. Madsen, Phys. Lett. *68B*, 55 (1977).
(46) R. E. Pixley and W. Benenson, Nucl. Phys. A *91*, 177 (1967).
(47) M. C. Bertin and R. E. Pixley, Nucl. Phys. A *150*, 247 (1970).
(48) A. B. Clegg, K. J. Foley, G. L. Salmon, and R. E. Segel, Proc. Phys. Soc. (London) *78*, 681 (1961).
(49) K. Strauch and F. Titus, Phys. Rev. *103*, 200 (1956).
(50) Y. S. Horowitz and R. E. Bell, Can. J. Phys. *48*, 201 (1970).
(51) F. Ajzenberg-Selove, Nucl. Phys. A *449*, 1 (1986).
(52) Ronald Murphy, Ph.D. thesis, University of Maryland, 1985.
(53) J. Meyer, Astrophys. J. Suppl. Ser. *57*, 173 (1985).
(54) D. W. Devins, D. L. Friesel, W. P. Jones, A. C. Attard, I. D. Svalbe, V. C. Officer, R. S. Henderson, B. M. Spicer, and G. G. Shute, Aust. J. Phys. *32*, 323 (1979).
(55) H. G. Pugh, D. L. Hendrie, M. Chabre, E. Boschitz, and I. E. McCarthy, Phys. Rev. *155*, 1054 (1967).

1. Report No. NASA TM-87787	2. Government Accession No.	3. Recipient's Catalog No.
4. Title and Subtitle Cross Sections for Production of the 15.10-MeV and Other Astrophysically Significant Gamma-Ray Lines Through Excitation and Spallation of ^{12}C and ^{16}O With Protons		5. Report Date September 1986 6. Performing Organization Code 682
7. Author(s) F.L. Lang, C.W. Werntz, C.J. Crannell, J.I. Trombka, and C.C. Chang		8. Performing Organization Report No. 86 B0418
9. Performing Organization Name and Address Goddard Space Flight Center Greenbelt, Maryland 20771		10. Work Unit No. 11. Contract or Grant No.
12. Sponsoring Agency Name and Address National Aeronautics and Space Administration Washington, DC 20546		13. Type of Report and Period Covered Technical Memorandum 14. Sponsoring Agency Code

15. Supplementary Notes

F.L. Lang and C.W. Werntz are working with Goddard Space Flight Center under grant NSG 5066 to The Catholic University of America

C. C. Chang is a faculty member at the University of Maryland.

16. Abstract

The ratio of the flux of 15.10-MeV gamma rays to the flux of 4.438-MeV gamma rays resulting from excitation of the corresponding states in ^{12}C is a sensitive measure of the spectrum of the exciting particles produced in solar flares and other cosmic sources. These gamma rays are produced predominantly by interactions with ^{12}C and ^{16}O, both of which are relatively abundant in the solar photosphere. Gamma ray production cross sections for proton interactions have been reported previously for all important channels except for the production of 15.10-MeV gamma rays from ^{16}O. The first reported measurement of the 15.10-MeV gamma ray production cross section from p + ^{16}O is presented here. The University of Maryland cyclotron was employed to produce 40-, 65-, and 85-MeV protons which interacted with CH_2 and BeO targets. The resultant gamma ray spectra were measured with a high-purity germanium semiconductor detector at 70, 90, 110, 125, and 140 degrees relative to the direction of the incident beam for each proton energy. Other gamma ray lines resulting from direct excitation and spallation reactions with ^{12}C and ^{16}O were observed as well, and their gamma ray production cross sections, several of which have not been reported previously, are presented. The results are compared with previously reported measurements, as available.

17. Key Words (Selected by Author(s))	18. Distribution Statement
Gamma Rays Nuclear Gamma-Ray Lines Solar Flare Gamma Rays	Unclassified—Unlimited Star Category 73

19. Security Classif. (of this report)	20. Security Classif. (of this page)	21. No. of Pages	22. Price*
Unclassified	Unclassified	44	A03

*For sale by the National Technical Information Service, Springfield, Virginia 22161

NASA-Langley, 1986

End of Document